NIST Technical Note 2059

NIST-NPL Bilateral Comparison of Guarded-Hot-Plate Laboratories from 20 °C to 160 °C

Robert R. Zarr
Jiyu Wu
Hung-kung Liu

This publication is available free of charge from:
https://doi.org/10.6028/NIST.TN.2059

NPL
National Physical Laboratory

NIST
National Institute of Standards and Technology
U.S. Department of Commerce

NIST Technical Note 2059

NIST-NPL Bilateral Comparison of Guarded-Hot-Plate Laboratories from 20 °C to 160 °C

Robert R. Zarr
Energy and Environment Division
Engineering Laboratory
National Institute of Standards and Technology

Jiyu Wu
Materials Characterisation Group
Department of Engineering
National Physical Laboratory

Hung-kung Liu
Statistical Engineering Division
Information Technology Laboratory
National Institute of Standards and Technology

This publication is available free of charge from:
https://doi.org/10.6028/NIST.TN.2059

January 2020

U.S. Department of Commerce
Wilbur L. Ross, Jr., Secretary

National Institute of Standards and Technology
Walter Copan, NIST Director and Undersecretary of Commerce for Standards and Technology

National Institute of Standards and Technology Technical Note 2059
Natl. Inst. Stand. Technol. Tech. Note 2059, 44 pages (January 2020)
CODEN: NTNOEF

This publication is available free of charge from:
https://doi.org/10.6028/NIST.TN.2059

Abstract

A bilateral study to compare guarded-hot-plate measurements at extended temperatures between laboratories at the National Institute of Standards and Technology (NIST) and the National Physical Laboratory (NPL) is presented. Measurements were conducted in accordance with standardized test methods (ISO 8302 or ASTM C 177) over a temperature range from 20 °C to 160 °C (293 K to 433 K). Following a blind round-robin format, specimens of nonwoven fibrous glass mat, approximately 22 mm thick and having a nominal bulk density of 200 $kg \cdot m^{-3}$, were prepared and studied. Results of the study show that the thermal conductivity measurements agree over the temperature range of interest to within ±1.0 %, or less. Consensus and individual laboratory fits to the data as a function of mean temperature are presented graphically. Sources of measurement variability are addressed.

Key words

Bilateral; Fibrous glass mat; Guarded hot plate; Industrial insulation; Interlaboratory comparison; Thermal conductivity; Thermal insulation; Uncertainty.

Table of Contents

1. Introduction 1
2. Specimens 1
2.1. Material 1
2.2. Preparation 2
2.3. Evaluation and Selection 4
3. Comparison Protocol 6
3.1. Test Conditions 7
3.2. Specimen Characterization 7
3.3. Guarded-hot-plate Measurements 7
4. Apparatus and Uncertainties 8
4.1. Test Method 8
4.2. NIST 9
4.3. NPL 11
4.4. Apparatus Comparison 13
4.5. Laboratory Uncertainty Budgets 14
5. Measurements 16
5.1. Specimen Bulk Density 17
5.2. Environmental Conditions 17
5.3. Guarded-Hot-Plate Measurement Results 17
6. Analysis 19
6.1. Graphical Exploration – Consensus Fit 19
6.2. Relative Deviations 20
6.3. Statistical (Type A) Significance 21
6.4. Engineering (Type A and Type B combined) Significance 22
6.5. Graphical Exploration – Individual Laboratory Fits 22
6.6. Confidence Ellipse 23
7. Discussion 24
7.1. Within-laboratory Effects 25
7.2. Between-laboratory Effects 26
8. Summary and Future Work 27
References 28
Appendix A: Comparison Protocol 29
Appendix B: Specimen Characteristics – Report Form 32
Appendix C: Guarded-Hot-Plate Measurements – Report Form 34
Appendix D: Environment Measurements – Report Form 36

List of Tables

Table 1. Test conditions and replicates. 7
Table 2. Summary of guarded-hot-plate apparatuses. 14
Table 3. NIST uncertainty budget at 20 °C. 15
Table 4. NPL uncertainty budget at 20 °C. 16
Table 5. Specimen characterization data prior to each run. 17
Table 6. Thermal conductivity data extracted from report forms in Appendix C. 18
Table 7. Linear fits for each laboratory. 23
Table 8. Original protocol test conditions 30

List of Figures

Fig. 1. TGA analysis of test samples of non-woven fibrous-glass mat. 2
Fig. 2. Test specimen configurations for NIST and NPL. 3
Fig. 3. Test specimens for NIST and NPL (faint square outline visible inside circular slab). . 3
Fig. 4. Test specimens in convection oven for conditioning at 475 °C for 24 h. 4
Fig. 5. Thermal resistance measurements for specimens 1 to 10 (2 and 8 highlighted). 5
Fig. 6. Mass measurements for specimens 1 to 10 (2 and 8 highlighted). 5
Fig. 7. Thermal conductivity of test specimens of non-woven fibrous glass mat as a function of bulk density (before and after heat treatment). 6
Fig. 8. Schematic of guarded-hot-plate apparatus: a) horizontal plates; b) vertical plates. 8
Fig. 9. NIST 500 mm diameter guarded-hot-plate apparatus: plates and edge guard (foreground), vacuum bell jar (background). 10
Fig. 10. Temperature sensor locations for NIST 500 mm diameter plates. 11
Fig. 11. Image of the NPL Guarded Hot-Plate for measuring thermal conductivity of insulation from –175°C to 160°C. 12
Fig. 12. Temperature sensor locations for NPL 305 mm by 305 mm plates (typical dimensions). 13
Fig. 13. Measured thermal conductivity of non-woven fibrous glass mat (205 $kg \cdot m^{-3}$) as a function of measured mean temperature. 19
Fig. 14. Scatter plot showing the relative deviations from the consensus line fit. 20
Fig. 15. Scatter plot showing the relative deviations from the consensus line fit with error bars representing the 95 % confidence interval based on the relative standard deviation from the consensus line fit (2 degrees of freedom). 21
Fig. 16. Scatter plot showing the relative deviations from the consensus line fit with error bars representing the expanded (k = 2) uncertainty interval reported by the laboratories. 22
Fig. 17. Measured thermal conductivity of non-woven fibrous glass mat (205 $kg \cdot m^{-3}$) as a function of measured mean temperature (individual linear fits). 23
Fig. 18. 95 % confidence ellipse plot. 24
Fig. 19. Cause-and-effect diagram for laboratory test result (λ_{exp}). 25
Fig. 20. Technical drawing of NIST and NPL specimens for waterjet cutting. 30
Fig. 21. NIST specimen data. 32
Fig. 22. NPL specimen data. 33
Fig. 23. NIST guarded-hot-plate measurement data. 34
Fig. 24. NPL guarded-hot-plate measurement data. 35
Fig. 25. NIST environmental data. 36
Fig. 26. NPL environmental data. 37

Glossary

A	specimen area normal to heat flux direction, m^2
CIPM	International Committee for Weights and Measures
CCT	Consultative Committee for Thermometry
c_i	sensitivity coefficient for an estimate x_i of input quantity X_i
GHP	guarded hot plate
GUM	Guide to the Expression of Uncertainty in Measurement
k	coverage factor
L	specimen thickness in the heat flow direction, m
n	number of observations
Q	time rate of one-dimensional heat flow through the metering area, W
q	one-dimensional heat flux through the metering area (Q/A), $W \cdot m^{-2}$
RH	relative humidity, %
SPRT	standard platinum resistance thermometer
s	standard deviation
TGA	thermal gravimetric analysis
Type A	evaluation of uncertainty by statistical analysis
Type B	evaluation of uncertainty by means other than statistical analysis
T_c	area-weighted temperature of specimen cold surface, °C or K
T_h	area-weighted temperature of specimen hot surface, °C or K
T_m	mean specimen temperature $(T_h + T_c)/2$, °C or K
t-value	critical value from Student's t distribution computed for a pivot value based on α
U	expanded uncertainty (coverage factor k equal to 2)
U_r	relative expanded uncertainty (coverage factor k equal to 2)
u_c	combined standard uncertainty (coverage factor k equal to 1)
u_i	standard uncertainty for an estimate x_i of input quantity X_i
X_i	input quantity
x_i	input estimate for an input quantity
ΔT	temperature difference $(T_h - T_c)$, K
Δy_{rel}	relative deviation
α	(statistical) significance level
δ_{rel}	relative deviation (residual)
ρ	bulk density, $kg \cdot m^{-3}$
λ	(apparent) thermal conductivity, $W \cdot m^{-1} \cdot K^{-1}$
$\lambda(T)$	functional relationship between thermal conductivity and temperature, $W \cdot m^{-1} \cdot K^{-1}$
λ_{exp}	experimental thermal conductivity, $W \cdot m^{-1} \cdot K^{-1}$
$\hat{\lambda}$	predicted thermal conductivity, $W \cdot m^{-1} \cdot K^{-1}$
v	degrees of freedom $(n - 1)$

Additional subscripts and superscripts

$\bar{}$	denotes sample mean
1,2	denotes cold plate 1 or 2, respectively
A,B	denotes Type A or Type B uncertainty evaluation, respectively
avg	denotes average value associated with cold plates 1 and 2

1. Introduction

The derived quantity thermal conductivity is a vital metric for the energy performance of building materials and, for analogous reasons, has a comparable status of importance for insulating materials intended for industrial applications. Mechanical insulation is utilized by diverse facilities including commercial buildings, power generation, petroleum, chemical, transportation, and shipbuilding industries, among others. The need for reliable thermal conductivity data for these types of insulation is important to designers and engineers of industrial facilities and is critical to insulation manufacturers as part of their quality assurance programs. Information for these thermal properties is also essential in establishing a fair competitive basis for domestic and international commerce. The accurate determination of thermal conductivity for industrial insulating materials, however, becomes quite challenging at elevated temperatures.

Recently, the National Institute of Standards and Technology (NIST) in the US and the National Physical Laboratory (NPL) in the UK completed a bilateral comparison of guarded-hot-plate laboratories investigating the thermal conductivity of an industrial insulation from 20 °C to 160 °C (293 K to 433 K). The objective of the investigation was to compare the state of the art between the laboratories from ambient to moderate temperatures. This study is considered a first step for subsequent explorations of thermal conductivity reference materials intended for temperatures up to 650 °C. The benefit of a bilateral comparison, in contrast to a comparison among several laboratories, permits a direct and, typically, a more thorough evaluation of the data obtained from the two laboratories. By examining comparison data from only two labs, subtle trends in the data become (more) noticeable that, otherwise, could be obscured when data from several laboratories are present.

In preparation for this comparison, the laboratory participants developed a detailed test protocol that included a careful evaluation of candidate materials and test specimens, and a comprehensive test report form. This bilateral comparison utilized a single pair of specimens of non-woven fibrous glass mat that was tested sequentially in a blind round-robin format, first by NIST and subsequently by NPL. Each laboratory agreed to send its test data to a statistician in the NIST Statistical Engineering Division who, upon agreement from both laboratory participants, released the data (presented herein) for review. This report describes the preparation and selection of test specimens, the test protocol, equipment, and measurement results. The data are reviewed graphically and physical processes to explain the behavior of the data are suggested. Recommendations for the development of high-temperature reference materials are given.

2. Specimens

2.1. Material

The specimens were prepared from commercially available non-woven fibrous-glass mat, composed of 100 % E glass (alkali-free borosilicate glass), and having approximate values for bulk density and thickness of 200 $kg \cdot m^{-3}$ and 22 mm, respectively. The insulating material, which is intended for industrial applications, consists of continuous glass filament needled together bonding the fibers mechanically. The fibers, because of their abrasive characteristics, were treated with a starch-oil emulsion by the vendor to facilitate fabrication. This coating was later removed by NIST by conditioning the test specimens at elevated temperature (Sec. 2.2).

The thermal stability of the material was initially investigated using thermal gravimetric analysis (TGA). Two small samples, having masses of 20.4 mg and 23.9 mg, were taken from the material and heated in a nitrogen atmosphere at a rate of 5 °C·min^{-1} to 700 °C. Prior to heating, the samples were maintained at 30 °C for 15 min. Figure 1 plots the mass change, in percent, as a function of temperature for the two small samples (identified as #1, #2). The main feature of interest in Fig. 1 is the very small mass loss, on the order of 0.6 % to 0.8 % over the large temperature range. The mass loss was, presumably, due to the desorption of water and decomposition of organic materials, i.e., the starch-oil emulsion. The reason for the small increase in Sample #1 near 250 °C is not known.

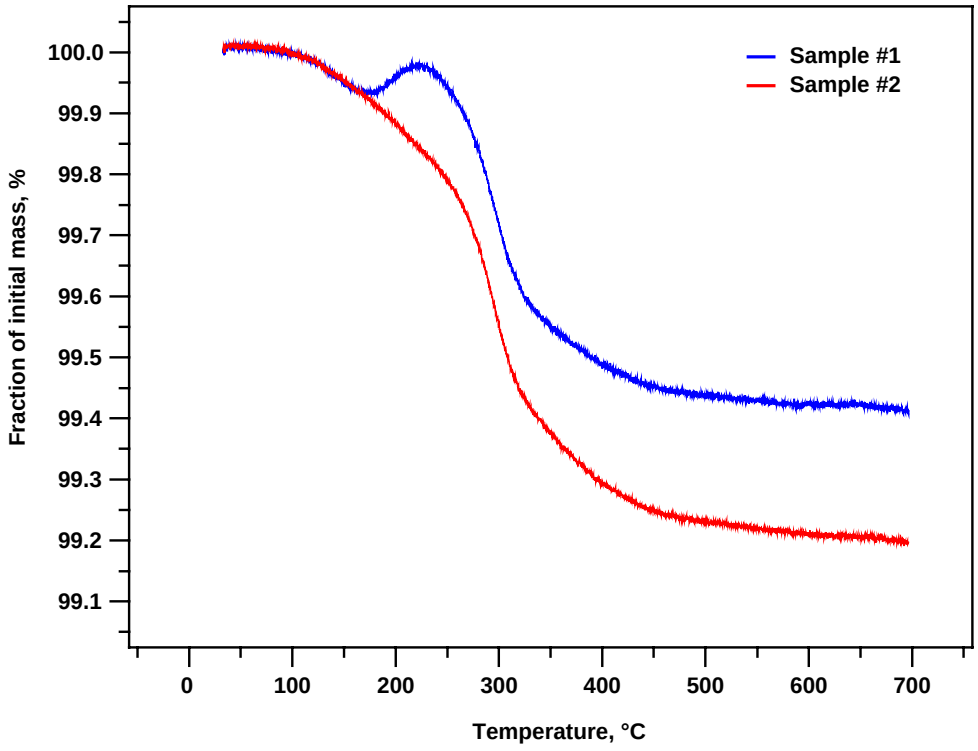

Fig. 1. TGA analysis of test samples of non-woven fibrous-glass mat.

2.2. Preparation

Figure 2 illustrates the comparative sizes of the thermal conductivity test specimens for the guarded-hot-plate apparatuses at NIST and NPL. Although three sets of specimens were initially considered (Fig. 2), the final number involved two guarded-hot-plate apparatus (circular geometry for NIST and square for NPL). NIST explored techniques for hand cutting the specimens, however, the complexity of inlaid patterns (Fig. 2), including their spacer cut-out profiles, proved too difficult to implement. Instead, the specimens were prepared by waterjet machining provided by a commercial vendor using water without added abrasives as the cutting fluid. The ten specimens were cut in pairs sequentially from a large roll of material acquired by NIST in 2007. Waterjet cutting under computer control is capable of accurate, intricate cuts in materials with minimum heating effects. Figure 3 is a photograph of the test specimens cut to final dimensions by waterjet machining. The outer circular slap represents the NIST specimen. The faint outline of the inner square NPL specimen is slightly visible.

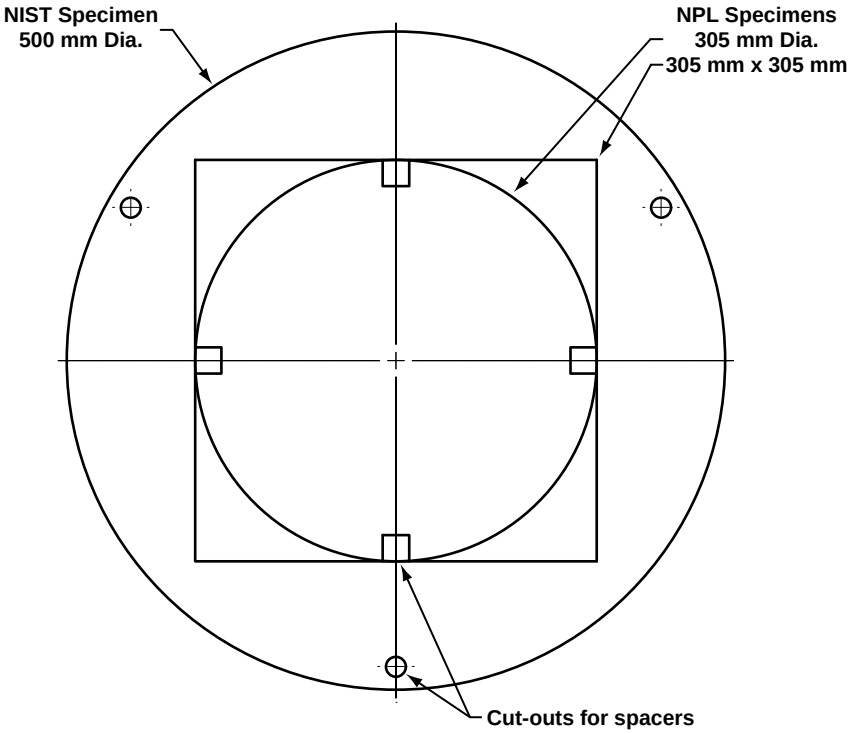

Fig. 2. Test specimen configurations for NIST and NPL.

Fig. 3. Test specimens for NIST and NPL (faint square outline visible inside circular slab).

To remove any organic material(s), the test specimens were heat treated in a large convection oven, shown in Fig. 4, over a period of three days. The air temperature in the oven was linearly ramped over a 24 h interval from room temperature to 475 °C, maintained at 475 °C for 24 h, and cooled to room conditions over the final 24 h.

Fig. 4. Test specimens in convection oven for conditioning at 475 °C for 24 h.

2.3. Evaluation and Selection

The evaluation of test specimens focused on two physical properties – specimen mass and, more importantly, thermal resistance – before and after heat treatment at 475 °C. The objective was to ascertain the best matched pair from the 10 specimens, that is, the two specimens nearest in agreement for both thermal resistance and specimen mass. Measurements of steady-state thermal transmission properties were conducted at NIST using a large heat-flow meter apparatus [1] at a mean temperature of 24 °C and a temperature difference of 22 K. The specimen masses were determined at NIST by gravimetric measurements.

Figure 5 plots the thermal resistance of the specimens before and after heat treatment denoted by triangle and square data points, respectively. The data are ranked by their initial measurements of thermal resistance (triangle data points). The average increase in thermal resistance for the 10 specimens was 3.7 %. As evident in Fig. 5, specimens 2 and 8 were among the closest in agreement for thermal resistance.

Figure 6 plots the corresponding mass loss of the specimens before and after heat treatment. The average loss for the 10 specimens was 1 %, which compares favorably with the TGA results from Fig. 1. The results of Fig. 6 show that specimens 2 and 8 are quite close in mass. Collectively, the results of Figs. 5 and 6 indicate that specimens 2 and 8 are the pair that was closest in in agreement for both thermal resistance and specimen mass. Consequently, specimens 2 and 8 were selected for the interlaboratory comparison.

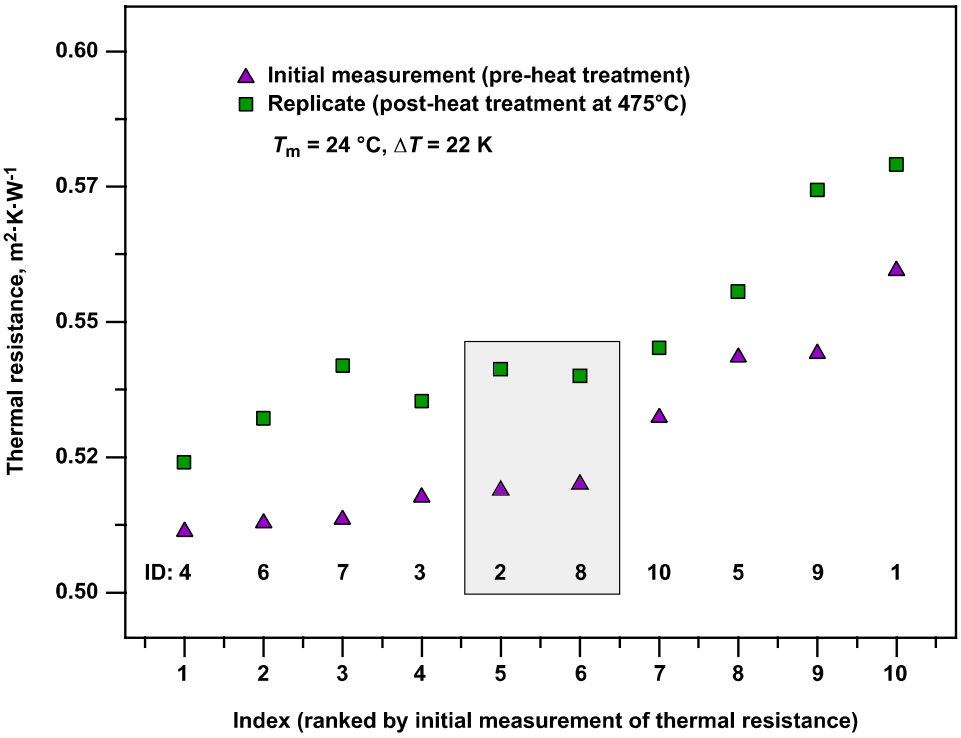

Fig. 5. Thermal resistance measurements for specimens 1 to 10 (2 and 8 highlighted).

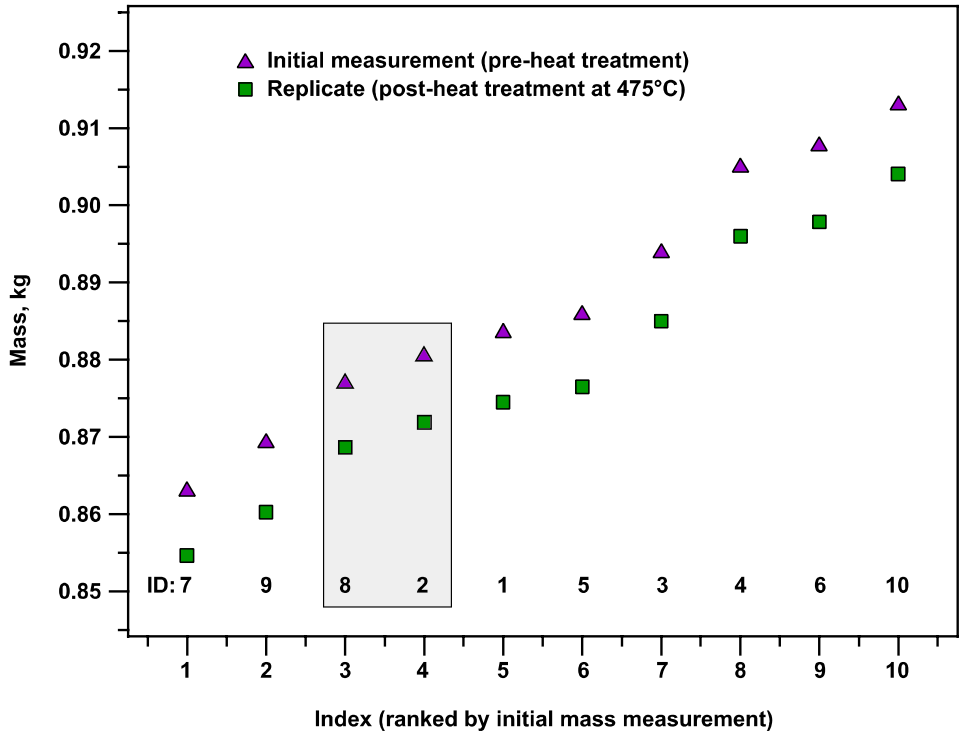

Fig. 6. Mass measurements for specimens 1 to 10 (2 and 8 highlighted).

Figure 7 plots the specimen thermal conductivity at 24 °C as a function of bulk density offering a supplementary assessment of the specimens. The horizontal lines represent the average thermal conductivity of the specimens before and after heat treatment (dashed and solid lines, respectively). Linear fitted lines for the data were investigated but, over the limited range of bulk density, the slopes were found to be small and statistically insignificant. As shown in Fig. 7, the bulk density of specimens 2 and 8 decreased by 4.2 %, but the thermal conductivity changed only slightly. This finding does not contradict the results of Fig. 5 because the thermal conductivity determination includes the effect of dimensional changes in the specimen thickness. In closing, Fig. 7 shows that specimens 2 and 8 are well matched in thermal conductivity and bulk density.

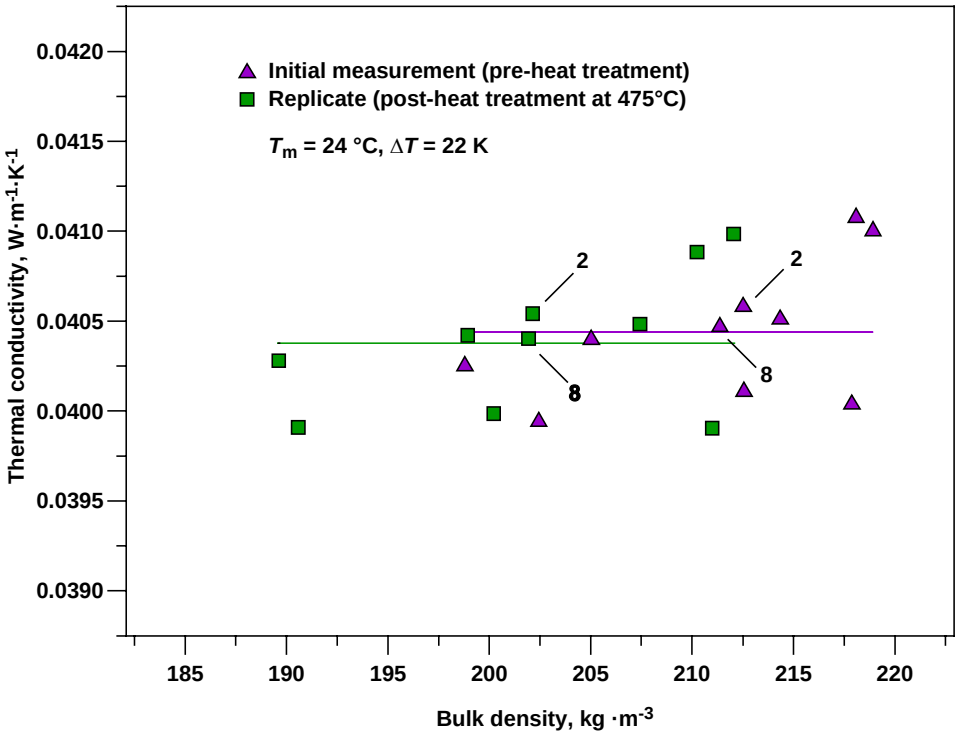

Fig. 7. Thermal conductivity of test specimens of non-woven fibrous glass mat as a function of bulk density (before and after heat treatment).

3. Comparison Protocol

The protocol document established by NIST and NPL for this comparison is provided in Appendix A. Development and approval of the protocol took place over several years due to changes in personnel at both NIST and NPL. The basic design of the comparison is that of a pilot study following a round-robin test program for a single pair of specimens. The guarded-hot-plate measurements were conducted first at NIST and subsequently at NPL. The specimen pair (2 and 8) were transported in a rugged flight case. It is important to emphasize that the participants followed a blind experimental protocol. The test results from each laboratory were submitted electronically to the NIST statistician and were only released after both data sets were received.

3.1. Test Conditions

Table 1 summarizes the measurement sequence, temperature settings, and the number of observations conducted per run at each temperature. Each laboratory participant conducted three runs at mean temperatures (T_m) from 20 °C to 160 °C for a total of 15 measurements. The observations at 90 °C were added later to corroborate the presence of curvature in the thermal conductivity data. The sequence order for T_m was deliberately not randomized due to practical considerations. The temperature difference (ΔT) was fixed at either 20 K or 25 K.

The purpose of conducting three runs was to determine the within-laboratory repeatability for each participant. Furthermore, every run was intended to be independent. To satisfy this requirement, the operator was requested, upon the completion of a run, to shut down their apparatus, remove the specimens and re-condition for 24 h prior to re-installation for the next run. Prior to each run, the specimens were conditioned at 23 °C ± 1 °C and 50 % RH ± 10 % RH for 24 h.

Table 1. Test conditions and replicates.

Sequence	T_m		ΔT	Observation per run		
	(°C)	(K)	(K)	1	2	3
1	20	293	20	1	1	1
2	40	313	20	1	1	1
3	90	363	25	1	1	1
4	140	413	25	1	1	1
5	160	433	25	1	1	1

3.2. Specimen Characterization

The laboratories determined the bulk density (ρ) of specimens 2 and 8 by gravimetric method prior to each run in their guarded-hot-plate apparatus. The final volume of the specimens was corrected by subtracting the spacer cut-out volumes to account for the minor volume of material removed for installation of the spacers (Fig. 2).

3.3. Guarded-hot-plate Measurements

The laboratories conducted the thermal conductivity measurements in accordance with their internal protocols based on standardized test method ISO 8302 [2] or ASTM C 177 [3]. Additional guidelines concerning specimen thickness and test order were agreed upon as described below and in Appendix A.

- *Spacers*: Both laboratory participants utilized rigid spacer stops located at the periphery of the specimens (Fig. 2). The spacer materials were fused-quartz and calcium silicate for NIST and NPL, respectively. Both laboratories corrected their in-situ thickness results for thermal expansion effects.
- *Test order*: Both laboratory participants conducted their measurements, for each run, in ascending order for the mean specimen temperature (Table 1).
- *Environment*: Both laboratory participants recorded their environmental conditions either near the specimens, that is, in the vacuum bell jar for NIST, or in the immediate laboratory enclosure for NPL.

4. Apparatus and Uncertainties

This section summarizes the test method and describes the guarded-hot-plate (GHP) apparatuses used in this comparison.

4.1. Test Method

Figure 8 illustrates the main components of a GHP apparatus designed for either: a) vertical or b) horizontal heat flow through the specimens. The typical arrangement, as shown in Fig. 8, utilizes parallel flat plates as constant temperature heat sources and sinks in contact with the surfaces of homogeneous specimens to establish a steady-state heat flux across the thickness dimension of the specimen. The central heating element of the apparatus (e.g., meter plate) is encompassed by a primary guard designed to promote one dimensional heat flow (Q) perpendicular to the plate surface in the central volume of the adjoining test specimens. The physical separation between the meter plate and guard plate components is designated the guard gap, or gap for short, and consists of an airspace.

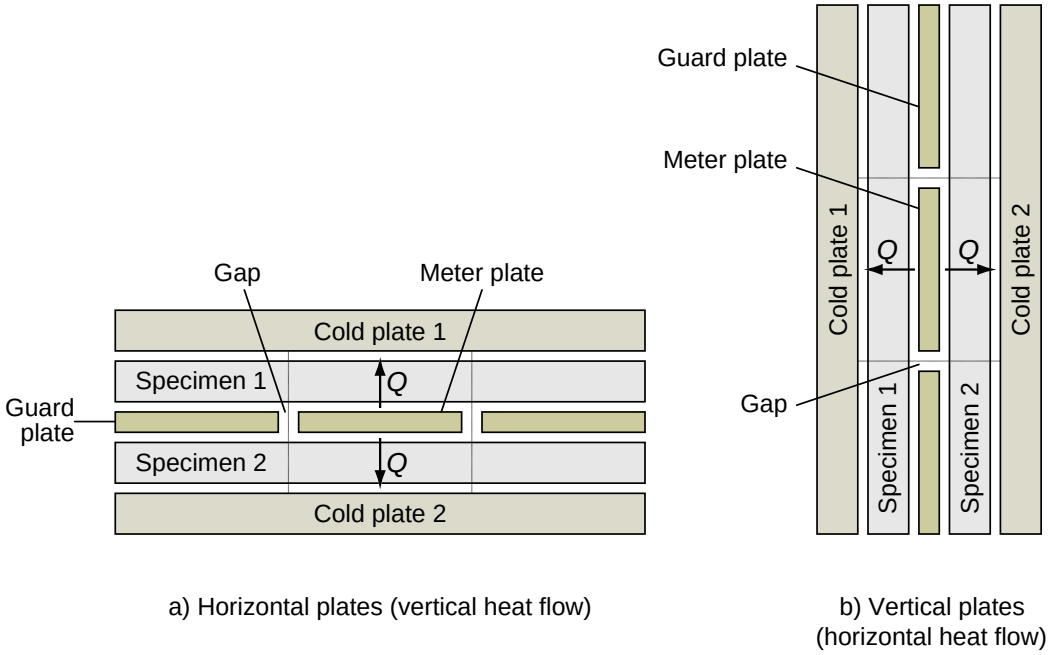

Fig. 8. Schematic of guarded-hot-plate apparatus: a) horizontal plates; b) vertical plates.

Standardized test methods [2-4] permit plate designs having either square or circular geometries and operation of the apparatus in either the double-sided (with two specimens) or single-sided (with a single specimen) modes of measurement. The double-sided mode requires that the cold plates operate at the same temperature; thus, the heat flow Q represents the measurement for the pair of specimens (Fig. 8). The guard plate is independently operated at the same temperature as the hot plate to minimize lateral heat flows.

The governing equation for the guarded-hot-plate method employs an algebraic form of the Fourier heat conduction equation. The thermal transmission calculations, based on heat flux measurements from the guarded-hot-plate apparatus, are implemented in accordance with Eq. (1) for double-sided operation.

$$\lambda_{\text{exp}} = \frac{Q\, L_{\text{avg}}}{2A\Delta T_{\text{avg}}} \tag{1}$$

The terms L_{avg} and ΔT_{avg} in Eq. (1) represent the average values associated with the pair of specimens 1 and 2 in Fig. 8. The $2A$ term in Eq. (1) represents heat flow through two surfaces of the metered area. Both laboratories corrected their metering areas for thermal expansion effects at a test temperature. Values of λ_{exp} are reported at the mean specimen temperature, T_{m}, given in Eq. (2).

$$T_{\text{m}} = \frac{T_{\text{h}} + T_{\text{c}}}{2} = \frac{T_{\text{h}} + \left(T_{\text{c1}} + T_{\text{c2}}\right)/2}{2} \tag{2}$$

The thermal transmission properties of heat insulators determined from standard test methods typically include multiple mechanisms of heat transfer, including conduction, radiation, and possibly convection. For that reason, some experimentalists will include the adjective "apparent" when describing the thermal conductivity of insulating materials. However, for brevity, the term thermal conductivity will be used in this report.

4.2. NIST

Figure 9 shows the GHP apparatus used in this comparison by NIST. The apparatus plates, shown in the vertical arrangement (illustrated schematically in Fig. 8b), are enclosed by a vacuum bell jar when under operation. The plates are commercially pure nickel and the working surfaces have been treated with a black ceramic coating to have a surface total emittance of 0.8. The surfaces in contact with the specimen metering area are flat to within 0.1 mm. The hot plate and cold plates are suspended from overhead rails and translate in the horizontal direction during installation of the specimen pair. A clamping force is transmitted axially to each cold plate by manual application, and an in-line load cell measures the applied loading (i.e., clamping pressure) during the test. The apparatus is described in detail in [5-6].

The hot plate is a monolithic assembly, 16.0 mm thick, consisting of a meter plate 200 mm in diameter and a co-planar, concentric guard plate 500 mm in diameter. The circular gap separating the meter plate and guard plate is 0.92 mm wide at the plate surface. The cross-sectional profile of the gap is diamond shaped to minimize lateral heat flow [5-6]. The temperature difference across the gap is measured by combining the outputs from two individual Type K twelve-junction thermopiles. Each thermopile is embedded on opposing surfaces of the hot plate.

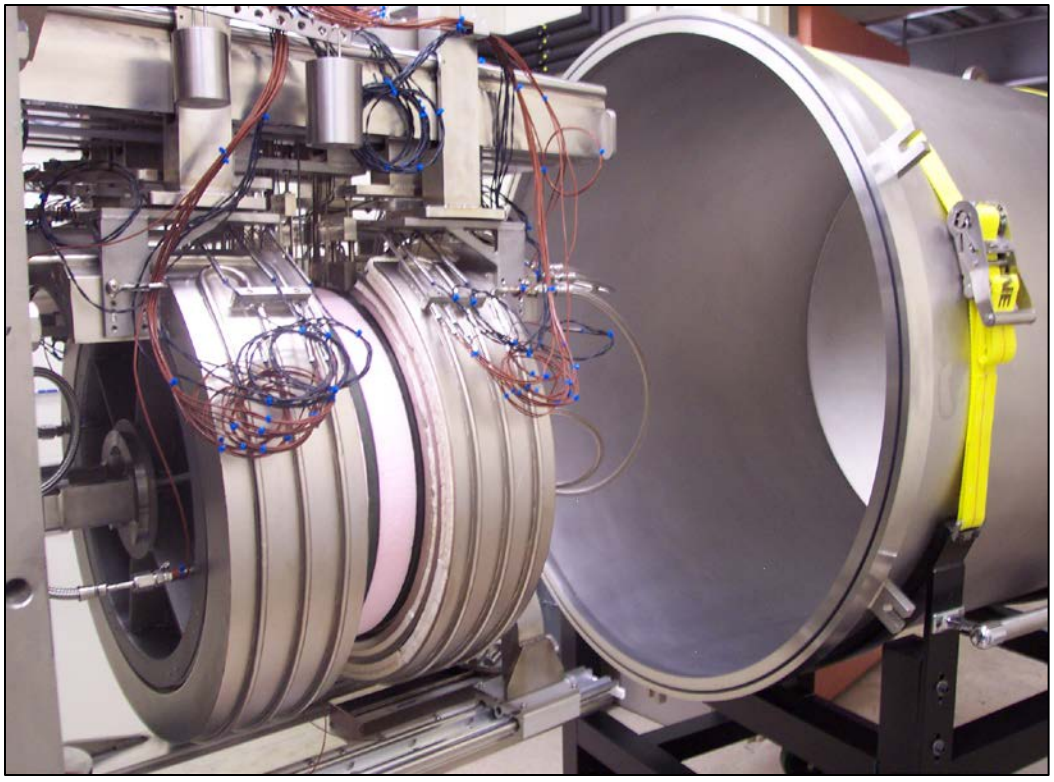

Fig. 9. NIST 500 mm diameter guarded-hot-plate apparatus: plates and edge guard (foreground), vacuum bell jar (background).

The metal-sheathed heaters for the hot plate are 3.2 mm in diameter and were custom manufactured using an internal bifilar design of nickel wires butt welded to gold (99.99 % nominal purity) wire leads. The heaters were formed such that the nickel-gold weld terminations were within 3 mm (or less) of the plate edge and the 2-to-4 wire transition of the meter-plate heater was within 1 mm of the centerline of the guard gap. After forming, the heaters were vacuum brazed in serpentine patterns at the midplane of the plate. The electrical resistance of the meter-plate heater at room temperature is approximately 3.3 Ω.

Each cold plate system is a multi-layered assembly consisting of the following components: thermometry plate; woven glass fabric; heater plate; microporous insulation; coolant plate; rigid alumina insulation; and, water-cooled back plate. For T_m equal to 20 °C and 40 °C (Table 2), a mixture of water and ethanol (70 %, 30 % by volume) was circulated through the coolant plates. For higher temperatures, dry air was circulated through the coolant plates. Temperature control of the thermometry plate was provided by the adjoining heater plate.

The primary temperature sensors installed in each plate are long-stem standard platinum resistance thermometers (SPRTs). The sensors have a 4-wire sensing element located within the first 50 mm of the sheath tip. The SPRT is placed in a well that is brazed at the midplane of the plate so that the sensing region resides in the geometric center of the plate as shown in Fig. 10. To check temperature uniformity of a plate, six Type N metal sheathed thermocouples, 1.6 mm in diameter, were brazed in the surface of each plate at the locations illustrated in Fig. 10.

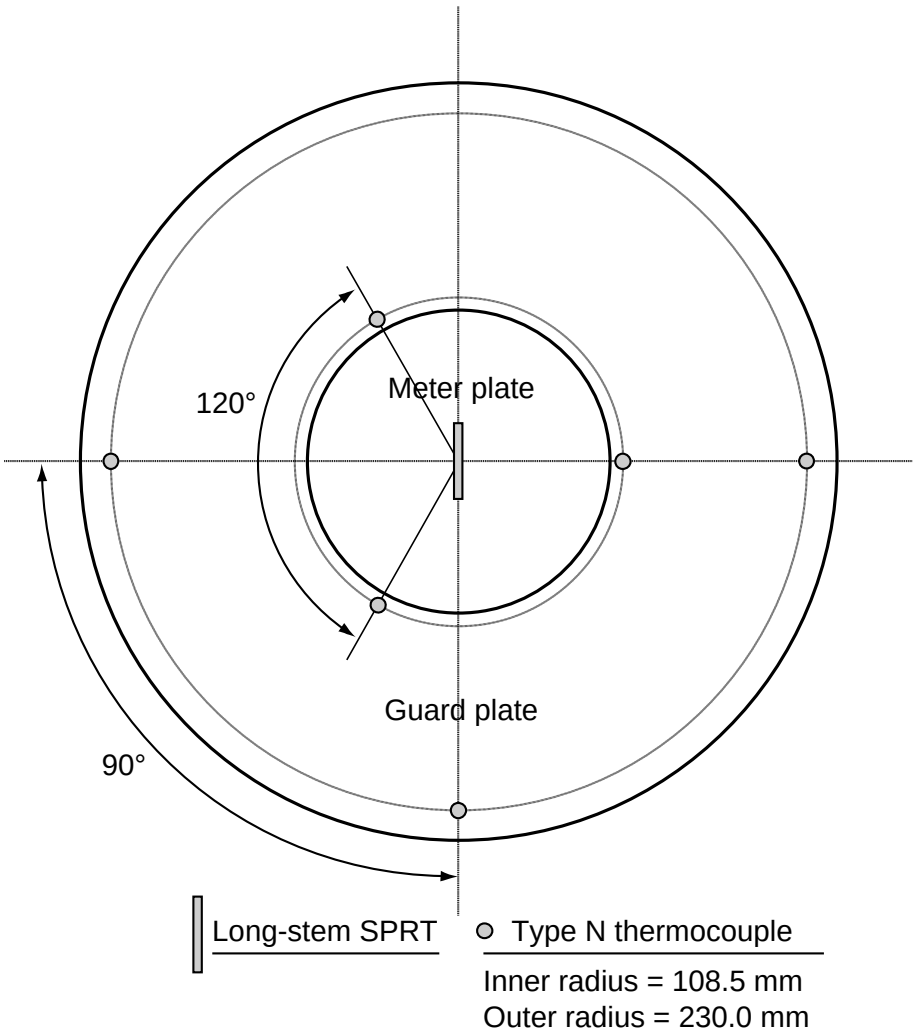

Fig. 10. Temperature sensor locations for NIST 500 mm diameter plates.

The meter plate electrical power is determined from the multiplicative product of the direct-current voltage and corresponding amperage of the circuit. The direct-current voltage across the meter-plate heater is measured by voltage taps welded to the heater leads in the center of the gap. The direct-current amperage is determined by measuring the voltage drop across a 0.1 Ω standard resistor placed in an oil bath at 25.0 °C and wired in series electrically with the meter plate heater.

4.3. NPL

Figure 11 shows the NPL GHP apparatus [7] used in this comparison. The NPL apparatus is a 305 mm by 305 mm double-sided guarded hot plate (NPL LTGHP) with a 150.5 mm by 150.5 mm physical centre area and an isothermal edge-guard. In the double specimen configuration, there is a specimen on either side of the heater-plate, and cold-plates on either side of the specimens. In this apparatus, the specimen is mounted horizontally (as illustrated schematically in Fig. 8a) within the apparatus, so that heat flows vertically from the heater-plate, through the specimens to the cold-plates. The apparatus was originally designed for measurements in the temperature range -175 °C to 50 °C and conformed to ISO 8302 [2] and EN 12667

[4]. The upper temperature limit has been recently extended to 160 °C. Its use is normally restricted to specimens up to 65 mm thick having a thermal conductivity up to 0.15 $W \cdot m^{-1} \cdot K^{-1}$ and thermal resistance down to 0.025 $m^2 \cdot K \cdot W^{-1}$.

Fig. 11. Image of the NPL Guarded Hot-Plate for measuring thermal conductivity of insulation from –175°C to 160°C.

The guarded heater plate was made of aluminium alloy and has lateral dimensions of 305 mm by 305 mm, with a central metering area of 152.5 mm by 152.5 mm and an air gap of 2 mm. Temperature balance between the metering area and lateral guard was maintained using the output of a 64-junction Type T thermopile with 32 junctions on each side to control the power supplied to the lateral guard heater. The two cold plates are each made from 30 mm thick copper, and their temperatures were regulated by a combination of fluid circulation and electrical heating. The surfaces of the guarded heater plate and cold surface plate had an estimated total hemispherical emittance of 0.9 and all the temperature sensors (Type T thermocouples) and electrical instruments used were calibrated with traceability to United Kingdom national standards. The plate/specimen stack is situated within an environmental chamber that consists of two chambers, one inside the other (Fig. 11). The air inside the inner chamber stabilizes at the temperature of the walls of the inner chamber and is maintained close to the mean specimen temperature. The apparatus has a compressive load system that incorporates a strain gauge, a motorized rotating screw lifting system, and an electronic control loop. The system maintains a compressive load (up to 2 kPa) on the specimen, as measured by the strain gauge, by raising or lowering the upper cold plate.

Figure 12 illustrates the lateral surface locations of the temperature sensors on the hot and cold plates. There are seven Type T thermocouples on each side of the guarded hot plate arranged so that five thermocouples are positioned within the metering area (i.e., meter plate) and two sensors are on the guard plate (Fig. 12a). For the cold plate, there are five Type T thermocouples arranged as shown in Fig. 12b on the surfaces in contact with the specimen.

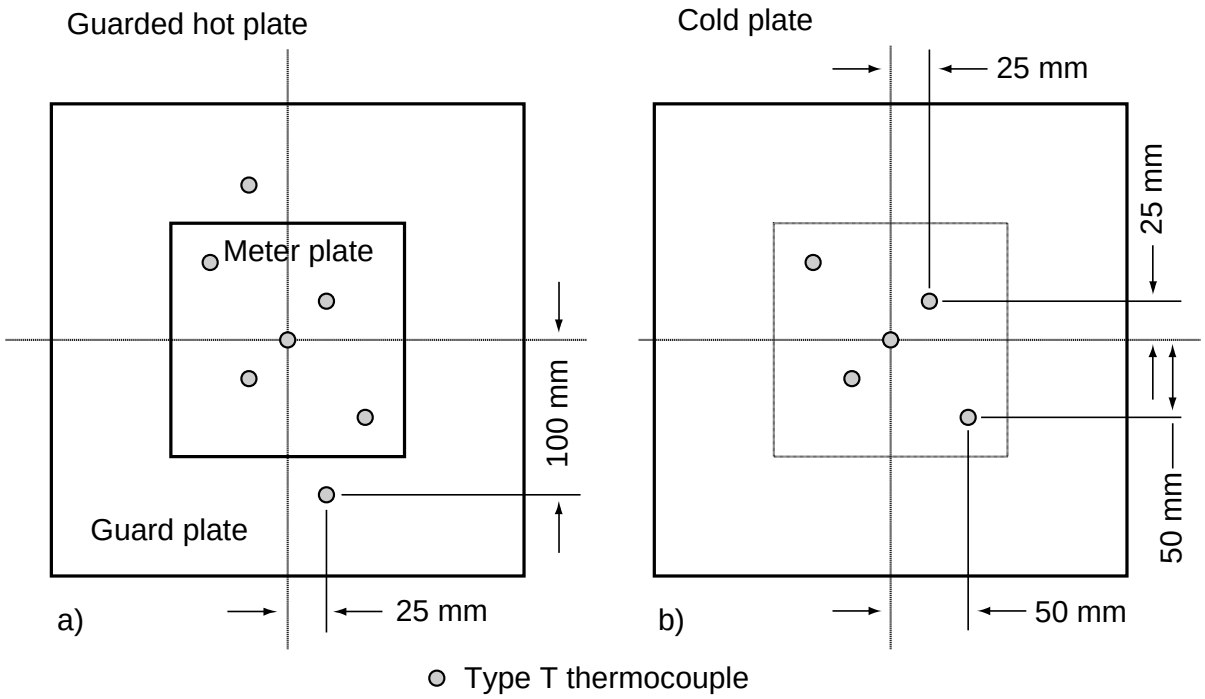

Fig. 12. Temperature sensor locations for NPL 305 mm by 305 mm plates (typical dimensions).

4.4. Apparatus Comparison

Table 2 summarizes the guarded-hot-plate apparatuses used by NIST and NPL in this study. The descriptions include 22 characteristics covering the size, shapes and orientations of plates, operation mode, and guarding, among other features of the equipment. Both laboratories have designed and constructed their guarded-hot-plate apparatus in-house [5-7].

As evident in Table 2, the apparatus are diverse in design and the few similarities that are prominent include: 1) two-sided operation mode; 2) comparable plate emittances; 3) same number of heaters in the meter plate; 4) same location of the voltage tap for the meter plate heater; 5) a guard gap consisting of an air space; and, 6) isothermal edge guard.

In contrast, there are major differences between the apparatus including: plate size, lateral plate guard ratio (2.5 versus 2.0), plate geometry (round versus square), orientation (horizontal versus vertical), guarding, and plate material (nickel versus aluminium). Additionally, the two apparatus utilize different configurations for the plate heaters and different types of primary temperature sensors, as well as a different number and type of edge guard temperature sensors.

Table 2. Summary of guarded-hot-plate apparatuses.

	NIST [5-6]	NPL [7]
Plate size	500 mm diameter	305 mm × 305 mm
Operation	2 sided	2 sided
Heat flow direction	horizontal	vertical
Plate material	nickel 201	aluminium alloy (heater plate), copper (cold plate)
Emittance	0.8	> 0.895
Meter plate size	200 mm diameter	150.5 mm × 150.5 mm
Meter plate sensor (number)	SPRT (1)	Type T (2×5)
Meter plate sensor location(s)	mid-plane center	surface grooves
Number heaters in plate	3	2
Number heaters in meter plate	1	1
Number heaters in guard plate	2	1
Heater type	metal sheathed	polyimide film
Heater active element	nickel 201	austenitic nickel-chromium
Heater configuration	labyrinth circular pattern	labyrinth rectangular pattern
Voltage tap location	4-wire, guard gap mid-point	4-wire, guard gap mid-point
Guard gap sensor type	Type K thermopile	Type T thermopile
Number of guard gap junctions	24 (12 each face)	64 (32 each face)
Guard gap material	airspace	airspace
Edge guard type	isothermal	isothermal
Edge guard sensor type	Type N	Type T
Number of edge guard sensors	12	1
Distance between plate and secondary guard	10 mm[a]	100 mm[b]

[a]Distance from plate edge to cylindrical edge guard
[b]Distance from plate edge to inside chamber wall

4.5. Laboratory Uncertainty Budgets

This section describes basic definitions, procedures, and formulae conforming to international guidelines [8] for evaluating the combined standard uncertainty, u_c, and expanded uncertainty, U, of λ_{exp} given by Eq. (1). The examples presented below abide by recently developed formats from an international comparison [9] of guarded-hot-plate apparatus organized under the auspices of the Consultative Committee for Thermometry (CCT), part of the International Committee for Weights and Measures (CIPM). The laboratory uncertainties, which include both Type A and Type B evaluations, are utilized in Sec. 6.4 to assess the engineering significance of the measured thermal conductivity data.

Under international guidelines [8], uncertainty components are classified by their method of evaluation. Type A evaluations are determined by statistical analysis of a series of independent observations. In this study, a Type A evaluation is useful for assessing dispersion about a consensus fit of the bilateral data (shown later in Sec. 6.3). In contrast, Type B evaluations are obtained from an assumed probability density function and can be based on information from previous measurements, calibration, experience, and manufacturer specifications, among other sources.

The combined standard uncertainty, $u_c(\lambda_{exp})$, is obtained by combining the individual standard uncertainties, u_i, by root sum of the squares [8]. Assuming the input quantities in Eq. (1) are uncorrelated, $u_c(\lambda_{exp})$ is the positive square root of the combined variance given by

$$u_c\left(\lambda_{exp}\right) = \sqrt{\sum_{i=1}^{N}\left[c_i u\left(x_i\right)\right]^2}, \tag{3}$$

where $u(x_i)$ are standard uncertainties of the input estimates for the input quantities, X_i, determined by each lab. The standard uncertainties, $u(x_i)$, are determined from either a Type A (statistical means) or Type B evaluation (non-statistical) described above.

The sensitivity coefficients, c_i, are partial derivatives and are evaluated at the input estimates x_i. Equation (4) derives the sensitivity coefficients for the input quantities in Eq. (1).

$$\begin{aligned} c_Q &= \frac{\partial\lambda}{\partial Q} = \frac{L}{2A\Delta T} = \frac{\lambda}{Q} \\ c_A &= \frac{\partial\lambda}{\partial A} = -\frac{QL}{2A^2\,\Delta T} = -\frac{\lambda}{A} \\ c_L &= \frac{\partial\lambda}{\partial L} = \frac{Q}{2A\Delta T} = \frac{\lambda}{L} \\ c_{\Delta T} &= \frac{\partial\lambda}{\partial\left(\Delta T\right)} = -\frac{QL}{2A\left(\Delta T\right)^2} = -\frac{\lambda}{\Delta T}. \end{aligned} \tag{4}$$

An example of the NIST uncertainty budget for thermal conductivity measurements of non-woven fibrous-glass mat specimen at 20 °C is shown in Table 3.

Table 3. NIST uncertainty budget at 20 °C.

Components	**Value**	u_i	c_i	$\lvert c_i \cdot u_i \rvert$
Heat flow Q	2.3580 W	1.26×10^{-4} W	0.01719 $m^{-1}\cdot K^{-1}$	2.17×10^{-6}
Metering area A	0.031730 m^2	2.32×10^{-6} m^2	-1.27711 $W\cdot m^{-3}\cdot K^{-1}$	2.97×10^{-6}
Specimen thickness L_{avg}	0.021772 m	2.45×10^{-6} m	1.86123 $W\cdot m^{-2}\cdot K^{-1}$	4.57×10^{-6}
Temperature diff. ΔT_{avg}	19.96 °C	2.91×10^{-2} K	-0.00203 $W\cdot m^{-1}\cdot K^{-2}$	5.90×10^{-5}
Thermal conductivity λ_{exp} *from Eq.* (1)	0.04051 $W\cdot m^{-1}\cdot K^{-1}$	*Combined standard uncertainty (k=1)* $(\Sigma\,\lvert c_i \cdot u_i\rvert^2)^{0.5}$		0.000059 $W\cdot m^{-1}\cdot K^{-1}$

Expressed as a percent, u_c from Table 3 is 0.15 %. The repeatability of the NIST guarded-hot-plate apparatus was determined from repeated measurements as a function of temperature. At 20 °C, the relative process standard deviation was 0.28 %. Summation of these relative values in quadrature yielded 0.32 % which was rounded, for convenience, to 0.5 % for this study. This process was repeated for the other mean temperatures. As shown in Sec. 5.3, the NIST uncertainties increased with temperature due to increasing variability in the replication data.

An example of the NPL uncertainty budget for non-woven fibrous-glass mat specimen measurements at 20 °C is shown in Table 4. The values for u_i are derived from an analysis of each element of the NPL LTGHP apparatus:

- u_Q includes resolution, calibration of electrical power measurement, metering/guard balance, metering/auxiliary balance and edge heat gains/losses.
- u_A includes resolution, calibration, alignment, and the uncertainty in the correction of the area due to thermal expansion effects.
- u_L includes resolution, calibration, parallelism, linearization, stability, and the uncertainty in the correction of specimen thickness due to thermal expansion effects.
- $u_{\Delta T}$ includes resolution, calibration, linearization and spread.

Table 4. NPL uncertainty budget at 20 °C.

Components	Value	u_i	c_i	$\lvert c_i \cdot u_i \rvert$
Heat flow Q	1.8524W	1.25×10^{-2} W	0.02222 $m^{-1} \cdot K^{-1}$	2.77×10^{-4}
Metering area A	0.023266 m^2	1.70×10^{-5} m^2	-1.76901 $W \cdot m^{-3} \cdot K^{-1}$	3.00×10^{-5}
Specimen thickness L_{avg}	0.020967 m	1.15×10^{-4} m	1.96298 $W \cdot m^{-2} \cdot K^{-1}$	2.26×10^{-4}
Temperature diff. ΔT_{avg}	20.28 K	9.71×10^{-2} K	-0.00203 $W \cdot m^{-1} \cdot K^{-2}$	1.97×10^{-4}
Thermal conductivity λ_{exp} *from Eq.* (1)	0.04116 $W \cdot m^{-1} \cdot K^{-1}$	*Combined standard uncertainty (k=1)* $(\Sigma \lvert c_i \cdot u_i \rvert^2)^{0.5}$		0.00041 $W \cdot m^{-1} \cdot K^{-1}$

The results of Tables 3 and 4 indicate that, although the method used to combine standard uncertainties by NIST and NPL are the same, the underlying methods to determine the standard uncertainties for the primary quantities (Q, A, L_{avg}, and ΔT_{avg}) are different. Moreover, the process standard deviation for NIST was significant, particularly at elevated temperatures. To examine these differences more rigorously, the methods used to determine sublevel component uncertainties, u_i, need to be investigated. Further work is suggested in this area for future comparisons.

The combined standard uncertainty, u_c, is taken to have a coverage factor of k equal to 1. For this comparison, however, it was decided to utilize an expanded uncertainty, U, which has a coverage factor of k equal to 2 defining an interval having a level of confidence of approximately 95 % [8].

$$U = k u_c = 2 u_c \tag{5}$$

The relative expanded uncertainty is given by

$$U_r = \frac{U}{\lambda_{exp}}. \tag{6}$$

The relative expanded uncertainties, expressed as a percent (%), were reported by both laboratories for each thermal conductivity measurement.

5. Measurements

This section provides a synopsis of the laboratory measurements including the bulk density measurements obtained prior to each run and the guarded hot plate measurements conducted

at the test conditions described in Table 1. Report copies of the laboratory measurements are provided in Appendices B through D. The compiled data and supplementary information are also available, in the form of zipped files, online [10].

5.1. Specimen Bulk Density

As described in 3.2, pre-and post-characterization of specimens 2 and 8 were conducted by each laboratory for each run in the guarded-hot-plate apparatus. These independent assessments checked for changes in the physical properties of the material which, in turn, could indicate potential complications in the thermal conductivity measurements. The pre-run examinations were conducted in accordance with internal laboratory protocols after the specimens were conditioned at 23 °C ± 1 °C and 50 % RH ± 10 % RH for 24 h.

Table 5 extracts and summarizes the pre-run data for thickness, clamping pressure, and bulk density (ρ) from Appendix B. Values of ρ did not change appreciably across runs for either laboratory. The last column, however, shows an overall decrease in the specimen bulk densities between the 500 mm diameter and the 305 mm by 305 mm specimens studied at NIST and NPL, respectively. The difference is indicative of the presence of a small within-specimen inhomogeneity in the material. The minor differences in bulk density, however, have a minimal effect on the thermal conductivity measurements as demonstrated by the heat-flow-meter measurements of the 10 specimens (Fig. 7).

Table 5. Specimen characterization data prior to each run.

Run	Specimen ID	Thickness (mm)		Clamping pressure (kPa)		ρ (kg·m^{-3})		Change in ρ (%)
		NIST	NPL	NIST	NPL	NIST	NPL	
1	2	21.33	21.17	0.84	0.25	208.1	200.7	-3.5
	8	20.93	20.80	0.84	0.25	211.3	205.3	-2.8
2	2	21.40	21.17	0.84	0.25	207.5	201.0	-3.1
	8	21.07	20.79	0.84	0.25	209.3	205.3	-1.9
3	2	21.33	21.17	0.84	0.25	208.1	200.7	-3.6
	8	20.97	20.80	0.84	0.25	211.0	205.2	-2.7

5.2. Environmental Conditions

During the guarded-hot-plate tests, the participants recorded the ambient conditions in their respective laboratories. Because of major differences in exactly how the secondary guards of the guarded-hot-plate apparatus are instrumented, the test protocol defined ambient data as either the adjacent region around the apparatus (i.e., the chamber surrounding the apparatus) or from within the laboratory module accommodating the apparatus. As a result, NIST reported data from within the vacuum bell jar surrounding the apparatus and NPL reported data from the laboratory module (Appendix D).

5.3. Guarded-Hot-Plate Measurement Results

Table 6 extracts the thermal conductivity data from each laboratory report in Appendix C and compiles the pertinent input and output data for side-by-side comparison. The final two columns in Table 6 summarize the relative expanded uncertainties, U_r, for each measurement. Test data for λ and U_r (last four columns) are examined graphically in Sec. 6. The NIST and NPL data for heat flux, q, differed by a factor of 2. The difference, however, did not affect the determination of λ. Future comparisons should clearly specify in the protocol how the quantity q is to be reported.

Table 6. Thermal conductivity data extracted from report forms in Appendix C.

Test No.	Nominal T_m (°C)	Nominal ΔT (K)	L[a] (mm) NIST	L[a] (mm) NPL	T_h (°C) NIST	T_h (°C) NPL	T_c (°C) NIST	T_c (°C) NPL	q (W·m^{-2}) NIST	q (W·m^{-2}) NPL	λ (W·m^{-1}·K^{-1}) NIST	λ (W·m^{-1}·K^{-1}) NPL	U_r(λ), k=2 (%) NIST	U_r(λ), k=2 (%) NPL
1	20	20	21.772	20.967	30.000	29.350	10.037	8.930	74.294	40.126	0.04051	0.04120	1.0	1.8
2	40	20	21.772	20.969	50.000	49.290	30.008	29.030	79.022	41.919	0.04303	0.04339	1.0	1.9
3	90	25	21.773	20.975	102.495	101.350	77.505	77.360	112.448	56.363	0.04898	0.04928	1.5	2.0
4	140	25	21.774	20.981	152.500	151.590	127.500	127.550	126.695	63.908	0.05517	0.05578	2.0	2.0
5	160	25	21.774	20.983	172.500	171.580	147.500	147.540	132.611	66.829	0.05775	0.05833	2.5	2.0
6	20	20	21.772	20.967	29.999	29.270	10.018	8.990	74.172	39.809	0.04041	0.04116	1.0	1.9
7	40	20	21.772	20.969	49.998	49.460	29.999	29.020	78.918	42.219	0.04296	0.04331	1.0	2.0
8	90	25	21.773	20.975	102.500	101.500	77.502	77.320	112.088	56.788	0.04881	0.04926	1.5	2.0
9	140	25	21.774	20.981	152.502	151.610	127.499	127.560	126.286	63.954	0.05499	0.05579	2.0	1.9
10	160	25	21.774	20.983	172.498	171.600	147.502	147.550	132.016	66.885	0.05750	0.05836	2.5	1.8
11	20	20	21.772	20.967	30.004	29.360	10.004	8.910	74.418	40.156	0.04051	0.04117	1.0	1.9
12	40	20	21.772	20.969	50.000	49.410	30.000	29.010	79.109	42.221	0.04306	0.04340	1.0	1.9
13	90	25	21.773	20.975	102.496	101.480	77.501	77.250	112.653	56.800	0.04906	0.04917	1.5	2.1
14	140	25	21.774	20.981	152.498	151.640	127.500	127.440	127.066	64.291	0.05534	0.05574	2.0	2.0
15	160	25	21.774	20.984	172.497	171.960	147.502	147.430	133.096	68.159	0.05797	0.05830	2.5	2.1

[a]In-situ measurement with rigid spacers corrected for thermal expansion effects

6. Analysis

This section examines the thermal conductivity measurements from both laboratories and is motivated by a central theme of the comparison; that is, how do the laboratories perform over the predetermined temperature range. The objective of the analysis addresses the underlying question of interest: What is the level of difference, if any, between the laboratories; and, if present, is the level significant? The technical approach focuses on the following analyses:

1. Graphical exploration of the data;
2. Assessment of the statistical (Type A) significance of the data; and,
3. Assessment of the engineering (Type A and Type B combined) significance of the data.

6.1. Graphical Exploration – Consensus Fit

A linear relationship between the measured thermal conductivity (λ_{exp}) and mean specimen temperature (T_m) was assumed and the data from both laboratories were fit to the linear model. The final fitted model is given in Eq. (7). The residual standard deviation of the consensus line fit is 0.000349 $W \cdot m^{-1} \cdot K^{-1}$ on 28 degrees of freedom.

$$\hat{\lambda} = 0.038325 + 1.2263 \times 10^{-4} T_m \qquad (7)$$

Figure 13 shows the scatter plot for λ_{exp} as a function of T_m. The data from NIST and NPL are color coded as shown in the legend.

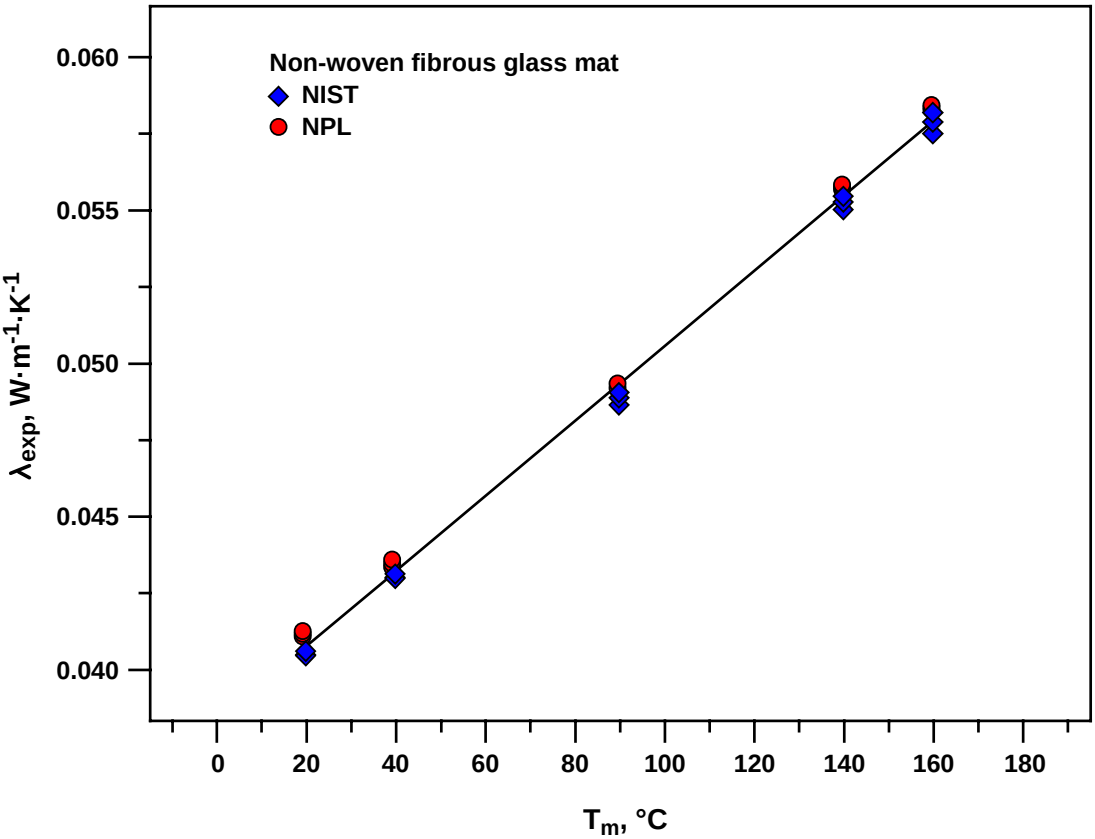

Fig. 13. Measured thermal conductivity of non-woven fibrous glass mat (205 $kg \cdot m^{-3}$) as a function of measured mean temperature.

6.2. Relative Deviations

The relative deviations from the fit in Eq. (7), which represent the relative vertical distance from the consensus line, were computed from Eq. (8):

$$\delta_{rel} = \frac{\lambda_{exp} - \hat{\lambda}}{\hat{\lambda}}, \tag{8}$$

where λ_{exp} is the experimental thermal conductivity from Eq. (1) and $\hat{\lambda}$ is the predicted value from Eq. (7). Figure 14 plots the relative deviations (often referred to as residuals) from the consensus line as a function of temperature. The individual runs (1, 2, 3) are coded as shown in the legend (solid line equals Run 1, dashed line equals Run 2, and dotted line equals Run 3).

Figure 14 reveals that most of the relative deviations are within ±0.01 (1 %) of the consensus fit and some are within ±0.005 (0.5 %) of the fit. The main conclusion from Fig. 14 is that the two laboratories do indeed behave differently – that is, there is a change in location relative to the consensus line. The NIST data suggest subtle non-linear behavior, and the individual runs behave systematically; the variation increases with temperature. The NPL data do not have systematic structure (i.e., more random behavior) but, in their entirety, exhibit curvature.

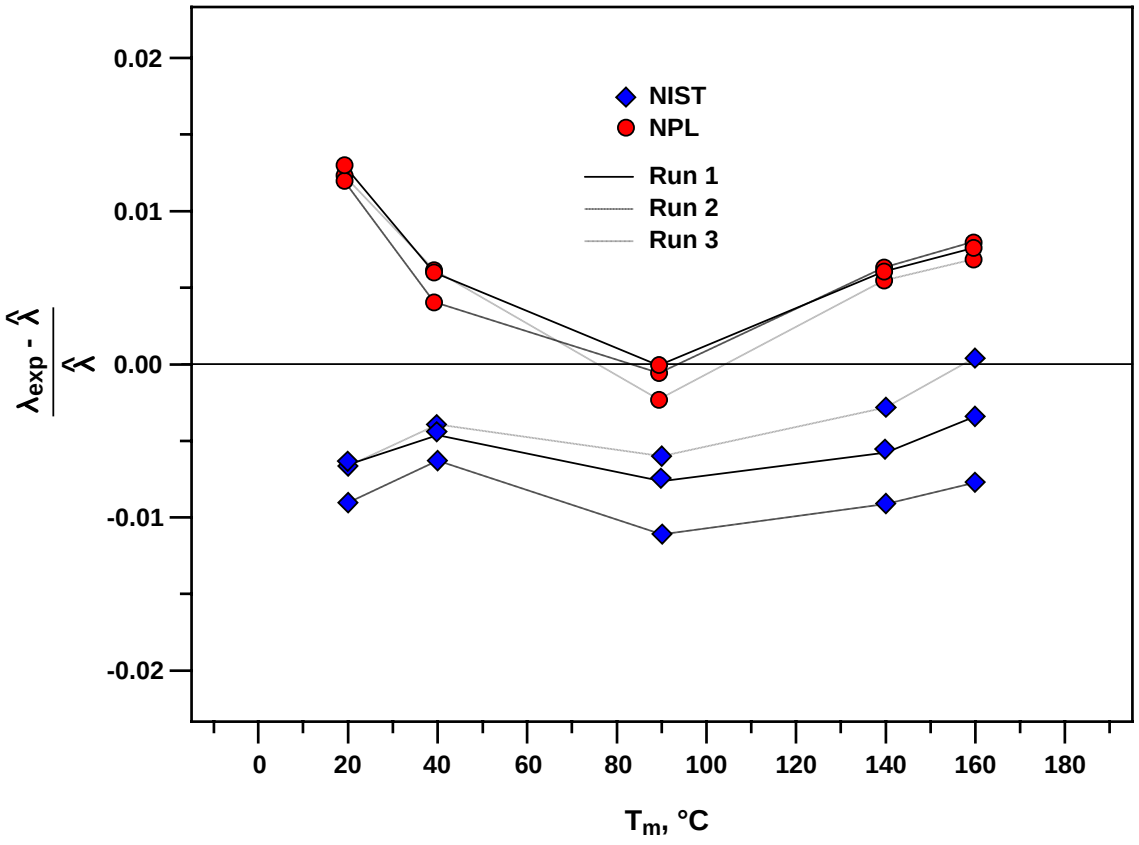

Fig. 14. Scatter plot showing the relative deviations from the consensus line fit.

6.3. Statistical (Type A) Significance

For each laboratory, Type A uncertainty intervals are constructed from confidence intervals centered on the mean of the three relative deviations at each value of temperature in Fig. 14. The confidence interval is constructed from the expression given in Eq. (9).

$$\Delta\bar{y}_{\text{rel}} \pm t_{\alpha/2}\left(\frac{s}{\sqrt{n}}\right), \tag{9}$$

where, for each temperature and each laboratory, s is the standard deviation of the 3 relative deviations. For a 95 % confidence interval where α equals 0.05 (two tail), the Student's critical t-value is computed for degrees of freedom (ν) = n – 1 = 2.

Figure 15 replots the relative deviations from Fig. 14 with error bars constructed from the 95 % confidence interval given in Eq. (9). From Fig. 15, we observe that the error bars overlap at 90 °C and 160 °C but not at the other temperatures. Based on the close relationship between confidence intervals and hypothesis testing, we conclude that, from a statistical (Type A) perspective, the deviations are different at the 0.05 level of significance.

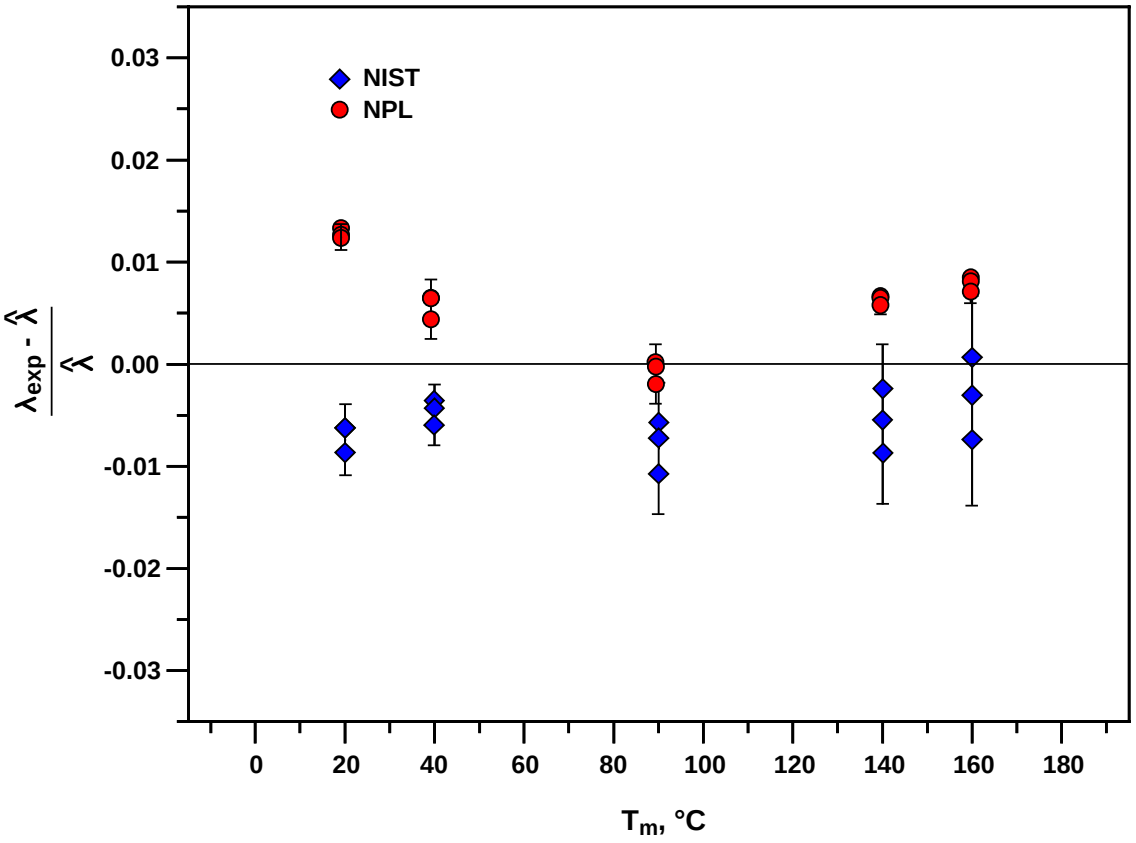

Fig. 15. Scatter plot showing the relative deviations from the consensus line fit with error bars representing the 95 % confidence interval based on the relative standard deviation from the consensus line fit (2 degrees of freedom).

6.4. Engineering (Type A and Type B Combined) Significance

Figure 16 replots the relative deviations from Fig. 14 with error bars constructed based on the expanded (Type A and Type B combined) uncertainty (k = 2) reported by the laboratories (Table 6). In contrast to Fig. 15, which examined the separation between labs based only on the bilateral comparison data, Fig. 16 incorporates supplementary laboratory uncertainties derived from data independent of this comparison (summarized in Table 6). We observe that, at every temperature, the error bars clearly overlap the respective laboratory data. Thus, we cannot conclude from an engineering viewpoint that the laboratories are significantly different. In other words, there is no detectable difference between the laboratories.

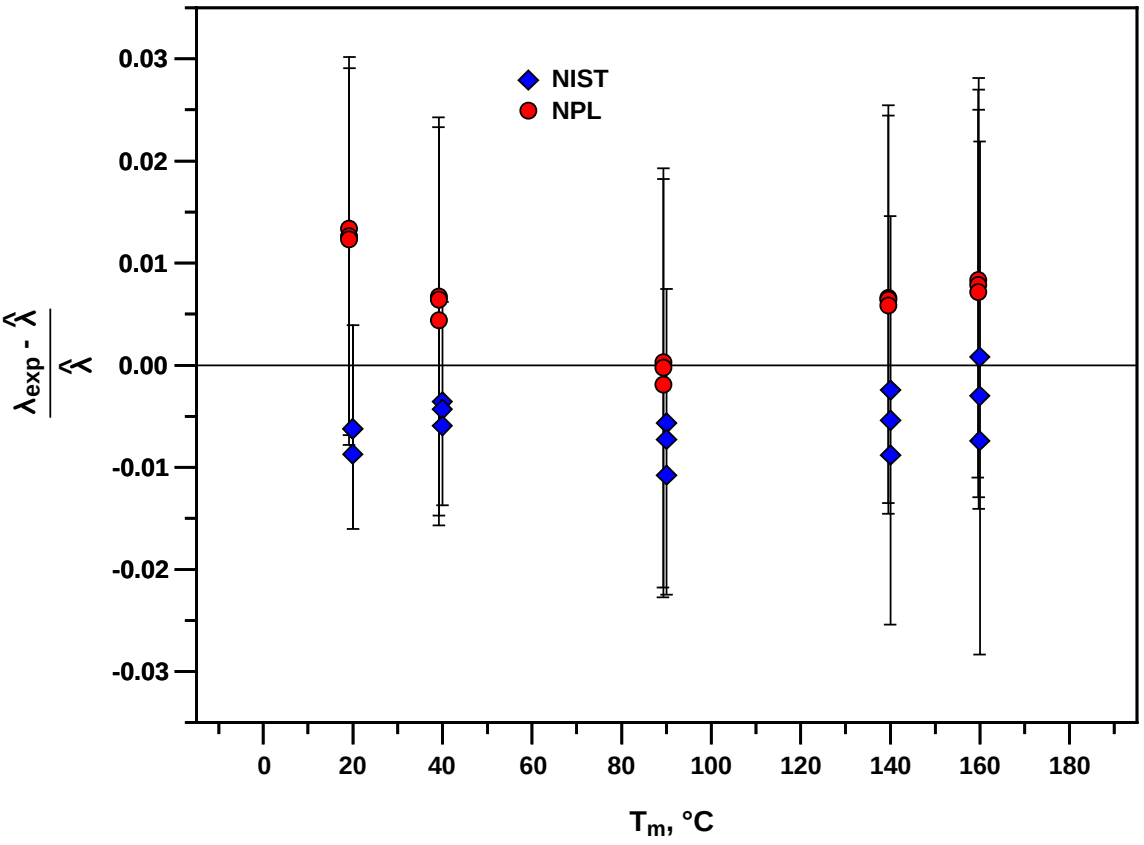

Fig. 16. Scatter plot showing the relative deviations from the consensus line fit with error bars representing the expanded (k = 2) uncertainty interval reported by the laboratories.

6.5. Graphical Exploration – Individual Laboratory Fits

In contrast to the consensus fit in 6.1, the thermal conductivity data from each laboratory were fitted to individual linear models summarized in Table 7. Although similar in concept to the original analysis, this approach seeks to answer a different, but related, question: are the two lines equivalent? Figure 17 replots the same data shown in Fig. 13 with individual linear fits for the NIST and NPL data.

Table 7. Linear fits for each laboratory.

	Intercept term		Temperature term	
Lab	Estimate	*s*	Estimate	*s*
NIST	0.03803	0.0000760	0.0001227	0.000000723
NPL	0.03861	0.000104	0.0001226	0.000000995

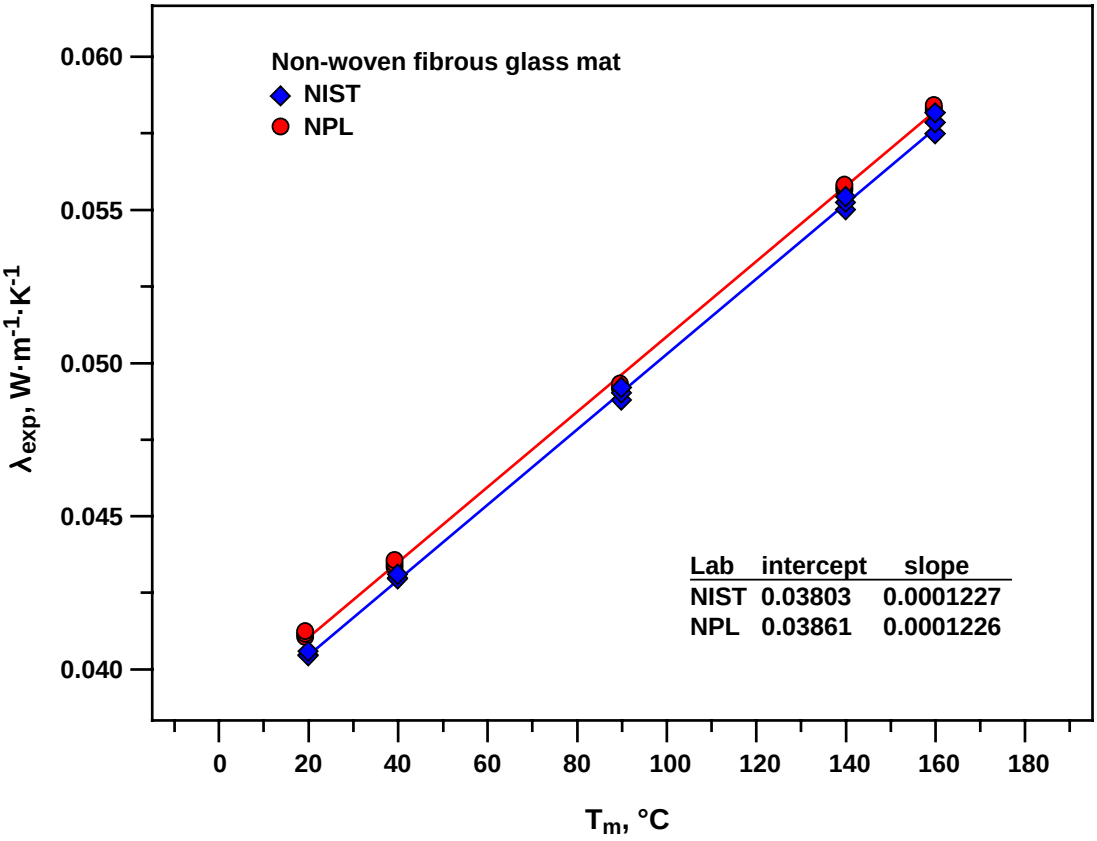

Fig. 17. Measured thermal conductivity of non-woven fibrous glass mat (205 kg·m^{-3}) as a function of measured mean temperature (individual linear fits).

6.6. Confidence Ellipse

Because lines are parametrized by intercept and slope, visually, we can represent each line by a single point on the slope-intercept plane as plotted in Fig. 18. The data are color coded following the same presentation as previous plots. The ellipse surrounding each point represents the region containing the true slope-intercept with 95 % confidence [11]. The angle of tilt indicates correlation between the fitted parameters of each line – slope and intercept. Examining Fig. 18 to compare the two lines, it is evident that both labs have very precise data. If, for example, the data were noisier, the ellipses would be more likely to overlap. It is clear that the slopes (vertical axis) for each lab overlap indicating that, from a statistical (Type A) perspective, the laboratory slopes are not different significantly. However, the intercepts (horizontal axis) do not overlap indicating that the laboratory intercepts are different significantly. In other words, a significant (Type A) offset is present.

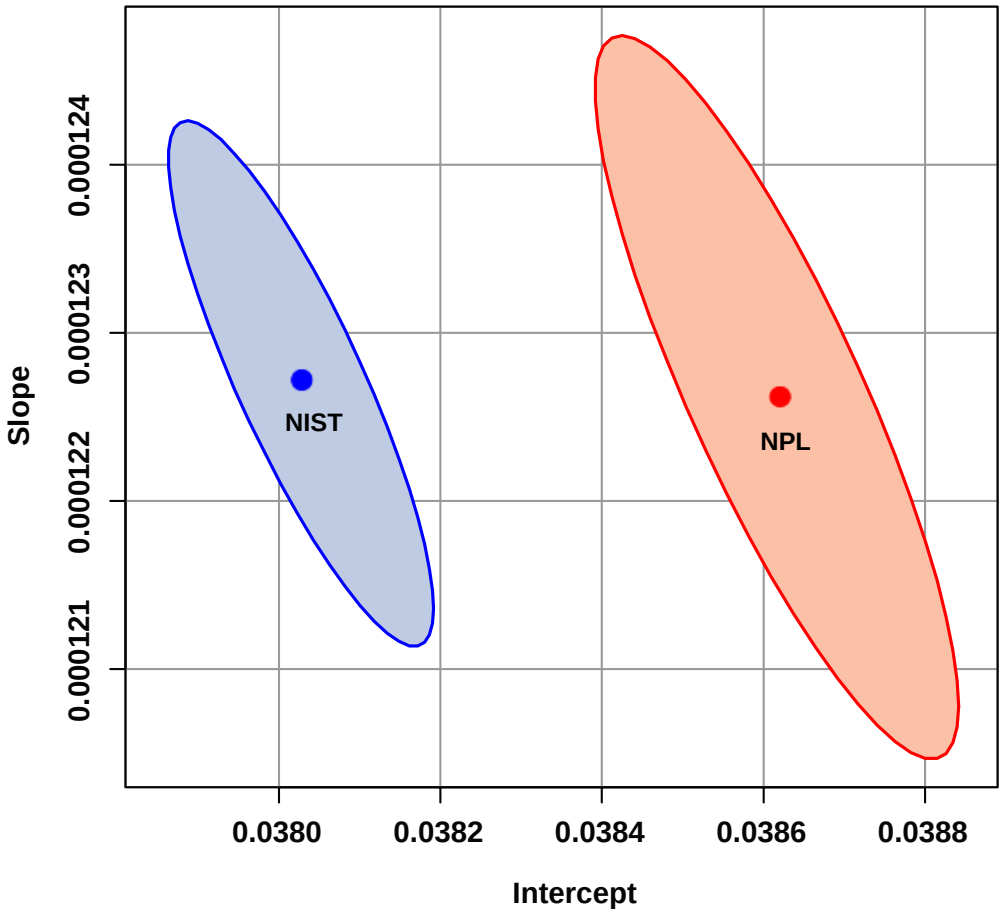

Fig. 18. 95 % confidence ellipse plot.

7. Discussion

The cause-and-effect diagram constructed in Fig. 19 shows six major causalities and identifies a few contributory factors that potentially affected the laboratory test result (λ_{exp}). The list of contributory factors is somewhat constrained by the scope of the comparison; for instance, only one material was studied in this comparison. Even so, there was a slight difference in the measured bulk densities, as evident in Table 5. This small difference is not believed to be a major effect as demonstrated in the heat-flow-meter data (Fig. 7) which shows that the thermal conductivity data are insensitive to bulk density for the range considered.

The other major factors – procedure, measurement, and equipment – are discussed in Sec. 7.1 and Sec. 7.2. The operator factor is set aside for the present study. The environmental factors are described in Appendix D. As a side note, it was realized during subsequent discussions by the laboratory participants that similar methods of cooling (Fig. 19) for the cold plates were utilized during the guarded-hot-plate tests. The effects of changing the coolants for active cooling during testing are discussed further in Sec. 7.1.

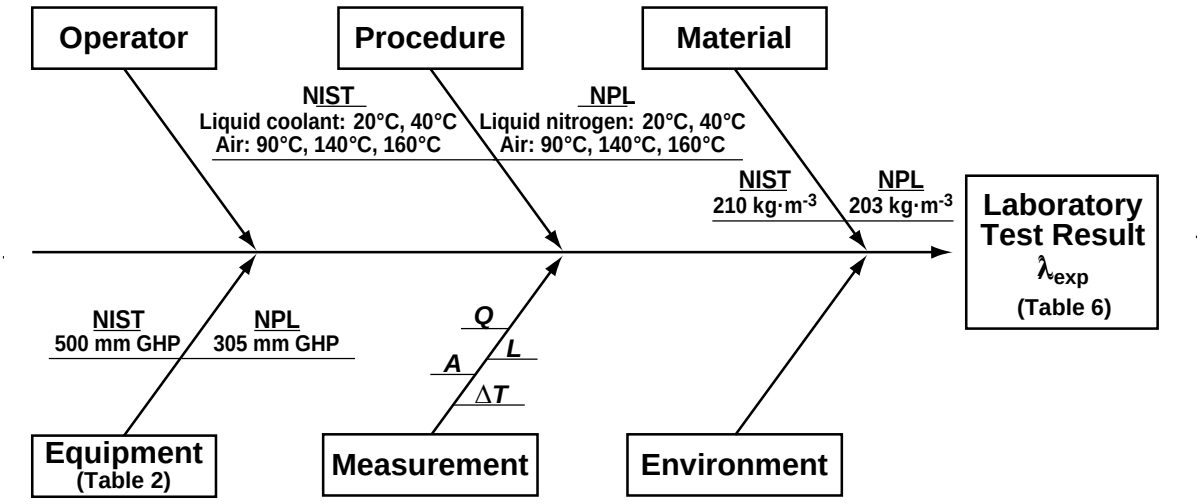

Fig. 19. Cause-and-effect diagram for laboratory test result (λ_{exp}).

7.1. Within-laboratory Effects

As clearly exhibited in the plot of relative deviations in Fig. 14, the within-laboratory variability is different for each laboratory. The within-lab effects for the NIST data points (diamond symbols), however, are more pronounced, particularly from 90 °C to 160 °C. An examination of internal NIST protocols, auxiliary test data in Appendix C, and subsequent measurement data obtained in a separate study identified two procedural factors and two equipment factors as likely sources for the variability exhibited in Fig. 14.

The initial level of variability observed at 20 °C and 40 °C is probably due to slight differences in the test setup for each run. To establish independent runs, the equipment was shutdown at the end of each run and the specimens were removed and re-conditioned. Prior to each run, the datum settings for the thickness and clamping load measurements were reset, potentially contributing to the initial level of variability. From 40 °C to 90 °C, there is also an interesting change in direction observed for each run. This subtle shift down coincided with a procedural adjustment for cooling the apparatus. At 20 °C and 40 °C, active cooling was provided by two refrigeration baths circulating a mixture of water and ethanol through the apparatus. At the completion of the 40 °C test, the mixture was drained, and active cooling for the higher temperatures was achieved by circulating air.

The increasing level of variability from 90 °C to 160 °C for the NIST data is not well understood at present. For insight, the auxiliary data presented in Appendix C on the temperature uniformity of the plates was examined. Figure 23 summarizes the standard deviations of the six thermocouples shown in Fig. 10 for the NIST hot plate and cold plates for each run. The temperature uniformity of the plates at 20 °C and 40 °C varied by about 0.1 K, or less. However, the variations for each plate increased dramatically from 90 °C to 160 °C. In the worst case, the variation of cold plate #2 at 160 °C was about 0.53 K. By comparison, the NPL plate uniformity in Fig. 24 for the thermocouples shown in Fig. 12 was generally on the order of 0.1 K, or less, over the entire temperature range.

The variations of the plate temperature uniformity were attributed, in part, to the plate thermal conductivity (aluminum and copper versus nickel) – the high thermal conductivity of the aluminum and copper plates in the NPL apparatus would enhance isothermal conditions. Another factor was recently discerned by a series of separate experiments conducted by NIST. That investigation revealed, for a fixed temperature, the variations of the plate temperatures decreased as the air pressure was decreased, indicating the probable presence of a convective loop within the apparatus. The effects of a convective loop would cause a vertical temperature gradient along the plates (Fig. 8b). Additional studies are recommended to verify the magnitude of this effect.

Although the within-lab effects for NPL are small, the NPL data points (circle symbols) in Fig. 14 exhibit curvature that may correlate to a procedural factor. At T_m of 20 °C and 40 °C, active cooling of the NPL apparatus was provided by circulating liquid nitrogen. For higher temperatures, active cooling was achieved by circulating compressed air. This procedural adjustment appears to have coincided with a change in the slope of the NPL data in Fig. 14.

7.2. Between-laboratory Effects

The response patterns between the laboratories observed in Fig. 14 appear quite consistent from run to run. The agreement between the laboratories is ± 1 %, or less, which is quite good over the temperature range of interest. It is somewhat surprising, however, that the minimum and maximum deviations between the laboratory data are at 90 °C and 20 °C, respectively. This trend departs from well-known assertions in guarded-hot-plate standards [2-4] that state that the test method is capable of measuring thermal conductivity to within ±2 % when the mean temperature is near room temperature and ±5 % over the entire operating range. The increasing trend observed in the deviations above 90 °C is possibly due to thermal radiation heat transfer. Further research is necessary to confirm this potential explanation.

In a recent bilateral comparison [12], the Laboratoire national de métrologie et d'essais (LNE) and NIST compared guarded-hot-plate data over a 17-year interval for two categories of insulation materials – fibrous and cellular polystyrene. Over a more limited temperature range of 7 °C to 47 °C (280 K to 320 K), the consistency in the data for fibrous and cellular insulating materials was on the order of ±1 % and ± 0.5 %, respectively. As was the case for this comparison, a graphical analysis revealed that the data for fibrous materials between LNE and NIST were mostly offset and parallel. Interestingly, in both studies, the NIST thermal conductivity data were typically lower than the data from the other national metrology institute.

An extensive analysis of causal factors in the LNE/NIST bilateral comparison [12] identified material composition (more specifically, anisotropic thermal conductivity properties), equipment design (e.g., lateral guarding), and their interaction as the most probable factors affecting the test results. In addition, it was noticed that for compressible materials, the usage of rigid spacer stops, as was done in this study, reduced the level of variability. Although this study was limited to a single fibrous material, it is plausible that a similar set of material causal factors affected the lab behavior between LNE and NIST, and between NIST and NPL.

8. Summary and Future Work

This bilateral study of guarded-hot-plate laboratories at NIST and NPL demonstrated that, over a temperature range of 20 °C to 160 °C (293 K to 433 K), the thermal conductivity test data for a non-woven fibrous-glass insulating material agreed to within ±1 %. The key finding is that, from an engineering perspective considering the combined laboratory uncertainties (both Type A and Type B), the analysis could not conclude that the laboratories were significantly different. The level of agreement in this study is well within uncertainty statements in guarded-hot-plate standards [2-4] of ±2 % when the mean temperature is near room temperature and ±5 % over the entire operating range.

A cause-and-effect analysis investigated possible factors that potentially affected the laboratory test results. The analysis identified a common factor between the labs that was procedural in classification. At temperatures below 90 °C, both laboratories employed active cooling using liquid coolants. In the case of NIST, a water/ethanol mixture was utilized and for NPL, liquid nitrogen. At 90 °C, and above, both laboratories circulated dry air for active cooling of the cold plates during testing. These changes in coolants appeared to result in changes in the behaviour of the laboratory thermal conductivity measurements. Further work, however, is needed to establish any causal relationship between differences in the coolants/procedures with deviations in the experimental results. The study also revealed the presence of lateral temperature variations in the NIST plates that may have contributed to increased variability in the thermal conductivity measurements at extended temperatures.

For the presentation of the uncertainty analyses, this study built upon current international guidelines for guarded-hot-plate comparisons. As part of the test protocol, the participants agreed to share their laboratory uncertainty budgets. Examples of uncertainty budgets conducted for 20 °C showed that, although the combined standard uncertainties were similar, the methods used to determine the uncertainties were different. For NIST, Type A evaluations predominated, and for NPL, the Type B evaluations tended to prevail. Further work is recommended in this area when conducting future bilateral comparisons.

This study is the first comparison of guarded-hot-plate laboratories from two national metrology institutes between Europe and the United States covering an extended temperature range. Corroboration of the guarded-hot-plate test method at extended temperatures is a critical step in the development of high-temperature thermal insulation reference materials. When properly prepared and conditioned (as was the case for this study), non-woven fibrous-glass mat is a candidate for further development. The next phase should focus on the robustness and long-term stability of the material.

Acknowledgments

The authors appreciate the guidance provided by William F. Guthrie, Chief NIST Statistical Engineering Division, in developing the test protocol used in this comparison. The test specimens of non-woven fibrous glass were cut under the supervision of Thomas Sterner at the LAI East facility, Division of LAI International, Inc. The authors thank the United Kingdom National Measurement System (NMS) for providing funding for NPL for this study. The NPL thermal conductivity measurements were conducted by Crispin Allen.

References

[1] ASTM International (2019) *C518-17 – Test Method for Steady-State Heat Thermal Transmission Properties by Means of the Heat Flow Meter Apparatus* (ASTM International, West Conshohocken, Pennsylvania).

[2] International Organization for Standardization (1991) *ISO 8302:1991 Thermal insulation – Determination of steady state thermal resistance and related properties – Guarded hot plate apparatus* (Geneva, Switzerland).

[3] ASTM International (2019) *C177-19 – Test Method for Steady-State Heat Flux Measurements and Thermal Transmission Properties by Means of the Guarded-Hot-Plate Apparatus* (ASTM International, West Conshohocken, Pennsylvania).

[4] European Committee for Standardization (2001) *EN 12667:2001 Thermal performance of building materials and products - Determination of thermal resistance by means of guarded hot plate and heat flow meter methods - Products of high and medium thermal resistance* (Brussels, Belgium).

[5] Flynn DR, Healy WM, Zarr RR (2006) High-temperature guarded hot plate apparatus: optimal locations of circular heaters. *Thermal Conductivity 28/Thermal Expansion 16*, Dinwiddie RB, White MA, McElroy DL, eds (DEStech Publications Inc. Lancaster, PA, USA), pp. 466-477.

[6] Zarr RR, Flynn DR, Hettenhouser JW, Brandenburg NJ, Healy WM (2006) Fabrication of a guarded-hot-plate apparatus for use over an extended temperature range and in a controlled gas environment. *Thermal Conductivity 28/Thermal Expansion 16*, Dinwiddie RB, White MA, McElroy DL, eds (DEStech Publications Inc. Lancaster, PA, USA), pp. 235-245.

[7] Stacey C, Salmon D, Simpkin A (2010) NPL guarded hot plate for measuring thermal conductivity of insulation from –175 °C to 50 °C. *Thermal Conductivity 30/Thermal Expansion 18*, Gaal DS, Gaal PS, eds (DEStech Publications Inc. Lancaster, PA, USA), pp. 671-681.

[8] International Bureau of Weights and Measures (2008) *JCGM 100:2008 Evaluation of measurement data – Guide to the Expression of Uncertainty in Measurement* (Paris, France).

[9] Hay B, Zarr R, Stacey C, Sokolov N, Lira-Cortes L, Zhang J, Hammerschmidt U, Filtz J-R, Joumani, T, Allard A (in preparation) Report on the CCT Supplementary comparison S2 on thermal conductivity measurements of insulating materials by guarded hot plate.

[10] Zarr RR, Wu J, Liu, HK (2019) Data from: Collaborative Guarded-Hot-Plate Tests between the National Institute of Standards and Technology and the National Physical Laboratory. National Institute of Standards and Technology (doi: 10.18434/M32106).

[11] Working H, Hotelling H (1929) Application of the theory of error to the interpretation of trends. *Journal of the American Statistical Association* 24(165A):73-85.

[12] Zarr RR, Guthrie WF, Hay B, Koenen A (2017) Collaborative Guarded-Hot-Plate Tests between the Laboratoire national de métrologie et d'essais and the National Institute of Standards and Technology. *Metrologia* 54(1):113-128.

Appendix A: Comparison Protocol

Prepared by: Robert Zarr and Will Guthrie, NIST, Jiyu Wu, and Clark Stacey, NPL
Final Revision: 23 November 2015 (Version 7)

A1. Objective: The objective of this pilot study is to compare the state-of art of thermal conductivity measurements between guarded-hot-plate apparatus at NPL and NIST.

A2 Participants: NIST, NPL

A3 Schedule

- *05 May 2011* Confirmation of participants
- *October 2011* Preparation of samples
- *23 May 2015* Agreements on schedule and measurement protocol
- *2017* Measurements will be carried out (measurement schedule will depend on the organization details)
- *2018-2019* Analysis of the results
- *TBD* Report

A4 Method: The thermal conductivity measurement will be carried out using a guarded-hot-plate apparatus according to ISO and/or ASTM test methods, as appropriate.

A5 Material

- Non-woven fibrous-glass blanket thermal insulation (100 % E-glass, mechanically bonded by needling process)
- Nominal bulk density (ρ): 200 $kg \cdot m^{-3}$
- Nominal thickness (L): 22 mm
- Nominal thermal conductivity (λ): 0.039 $W \cdot m^{-1} \cdot K^{-1}$ at mean temperature (T_m) of 24 °C
- Maximum service temperature: 538 °C (1000 °F)

A6 Specimens

- 10 specimens cut for multiple plate sizes (Fig. 20) by waterjet (NIST)
- 10 specimens conditioned (Fig. 2) in a convection oven at 475 °C for 24 h (NIST).
- Select 2 specimens (1 pair) matched for bulk density, thickness, and thermal resistance (NIST/NPL)
- Specimen pair designated as A and B (NIST/NPL)
- NIST will determine spacer lengths for specimens A and B and transmit length to NPL

A7 Protocol

- Participants complete the electronic data sheet *"GHP_Inter-Lab_NPL_NIST_ReportFormVer10.xlsx"* by entering data in the following workbook tabs.
    - Apparatus
    - Specimens
    - Measurements
    - Environmental

Appendix A

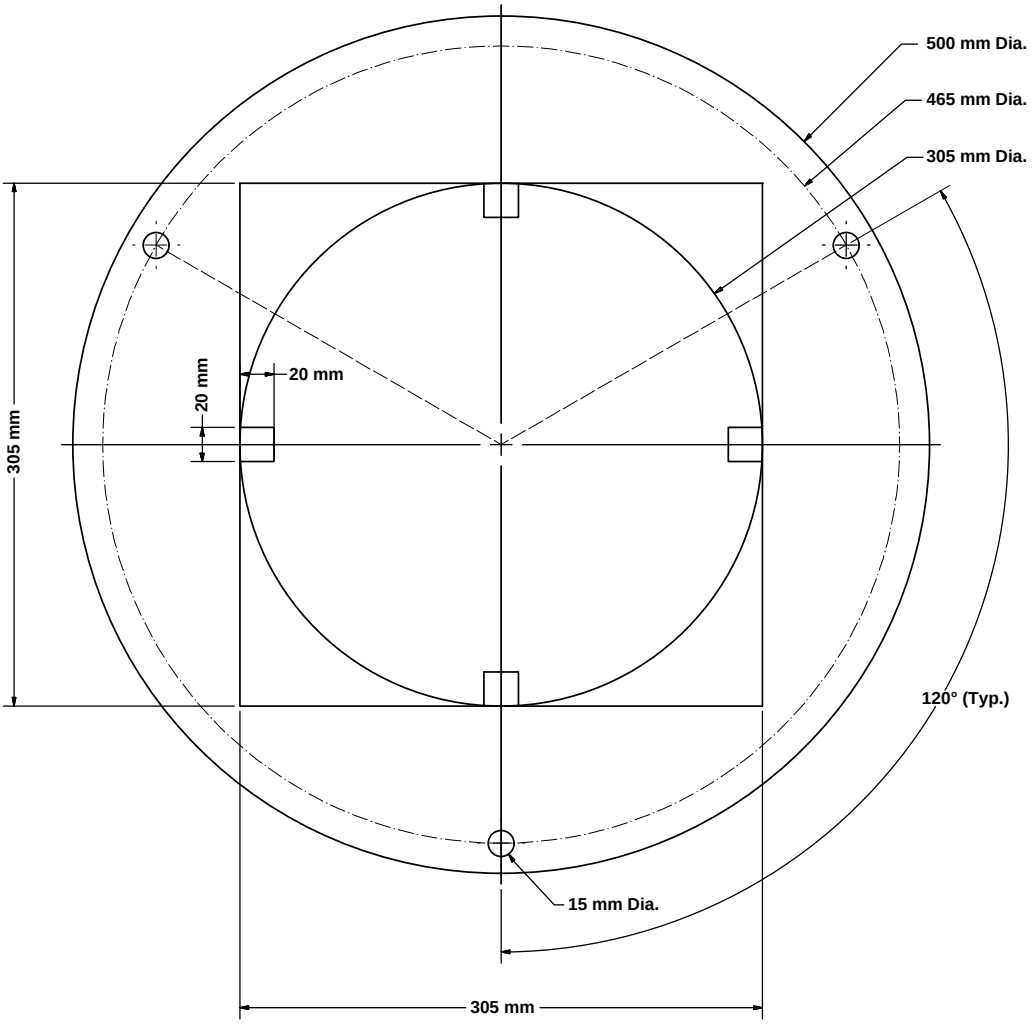

Fig. 20. Technical drawing of NIST and NPL specimens for waterjet cutting.

- **Test conditions**: Participants conduct 3 separate runs of guarded-hot-plate measurements at the temperature conditions summarized in Table 7.

Table 8. Original protocol test conditions

T_m		ΔT
(°C)	(K)	(K)
20	293	20
40	313	20
140	413	25
160	433	25

- **Specimen characteristics**: Participants determine the specimen characteristics before and after each run according to their internal laboratory protocols following the guidelines below:
    - Prior to a Run#1, condition the specimens at 23 °C ± 1°C, 50 % RH ± 10 % RH for 24 h.
    - After conditioning, determine specimen(s) A and/or B lateral dimensions (diameter or length and width).
    - After conditioning, determine the thickness of specimen(s) A and/or B under compressed load. Weigh specimen(s) A and/or B. Determine the bulk density (ρ) of specimen(s) A and/or B. The density determination excludes the insulation material to be removed for insertion of the spacers. Dimensional measurements of openings are to be measured and retained by each laboratory.
    - After each run (#1 thru #3), remove the specimen(s) from the apparatus and condition the specimens at 23 °C ± 1°C, 50 % RH ± 10 % RH for 24 h.
    - Repeat the dimensional/mass measurements (above) and re-compute the bulk density.
    - Complete the SPECIMEN CHARACTERISTICS section of the Measurements tab.

- **Guarded hot plate measurements**: Participants determine the thermal conductivity of the specimen(s) according to their internal laboratory protocols following the guidelines below:
    - **Specimen thickness:** The specimen thickness is determined using spacer stops placed between the apparatus plates. The spacer stops can be fabricated from either calcium silicate or fused quartz. The specimen thickness shall be corrected for thermal expansion effects of the spacer material.
    - **Clamping pressure (optional):** The clamping pressure can be recorded by each laboratory for their own purposes.
    - **Thermal conductivity measurements:** The thermal conductivity measurements are conducted at temperature conditions specified in Table 7 in ascending order (i.e., from lowest to highest value of T_m). The measurements are performed according to ISO 8302 or ASTM C 177.
    - Complete the GUARDED HOT PLATE MEASUREMENTS section of the Measurements tab.
    - Complete the MEASUREMENT ENVIRONMENT CONDITIONS section of the Environmental tab (averages of final steady-state period).

A8 Measurement Results

- The results of this comparison will be analysed by the NIST Statistical Division and discussed among the participants.
- The results of this comparison will be published only after agreement of all participants.
- The participants agree to share their uncertainty budgets. The complete details of the uncertainty budgets will not be published.

Appendix B: Specimen Characteristics – Report Form

LABORATORY:	NIST
APPARATUS:	500 mm guarded-hot-plate
MATERIAL:	non-woven fibrous-glass blanket

SPECIMEN CHARACTERISTICS		Actual conditions:					Spacer openings: NIST					REMARKS
	ID	Date of measurement	Thickness (mm)	Comp.Press. (kPa)	Diameter (mm)	Mass (kg)	Diameter #1 (mm)	Diameter #2 (mm)	Diameter #3 (mm)	Vol.$_{meas.}$ (m^3)	Bulk density ($kg{\cdot}m^{-3}$)	
Specimen A (before Run 1)	2	2016-Feb-05	21.33	0.84	500.00	0.8692	14.0	14.0	14.5	0.00001009	208.1	23°C, 45% RH, 27.3 h
Specimen B (before Run 1)	8	2016-Feb-05	20.93	0.84	500.00	0.8661	14.0	14.0	14.0	0.00000966	211.3	23°C, 45% RH, 27.3 h
Specimen A (after Run 1)	2	2016-Feb-18	21.41	0.84	500.00	0.8688	14.0	15.0	14.5	0.00001062	207.2	post-test
Specimen B (after Run 1)	8	2016-Feb-18	20.98	0.84	500.00	0.8658	14.0	14.0	14.0	0.00000969	210.7	post-test
Specimen A (before Run 2)	2	2016-Feb-19	21.40	0.84	499.75	0.8689	14.0	14.0	14.0	0.00000988	207.5	23°C, 45% RH, 27.0 h
Specimen B (before Run 2)	8	2016-Feb-19	21.07	0.84	500.50	0.8658	14.0	14.0	14.0	0.00000973	209.3	23°C, 45% RH, 27.0 h
Specimen A (after Run 2)	2	2016-Mar-01	21.34	0.84	499.50	0.8688	14.0	14.0	14.0	0.00000985	208.3	post-test
Specimen B (after Run 2)	8	2016-Mar-01	20.94	0.84	500.00	0.8656	14.0	14.0	14.0	0.00000967	211.0	post-test
Specimen A (before Run 3)	2	2016-Mar-02	21.33	0.84	499.75	0.8688	14.0	14.0	14.0	0.00000985	208.1	23°C, 45% RH, 27.4 h
Specimen B (before Run 3)	8	2016-Mar-02	20.97	0.84	499.75	0.8656	14.0	14.0	14.0	0.00000968	211.0	23°C, 45% RH, 27.4 h
Specimen A (after Run 3)	2	2016-Mar-14	21.19	0.84	500.00	0.8687	14.0	14.0	14.0	0.00000978	209.3	post-test
Specimen B (after Run 3)	8	2016-Mar-14	20.95	0.84	500.00	0.8654	14.0	14.0	14.0	0.00000968	210.8	post-test

Fig. 21. NIST specimen data.

Appendix B

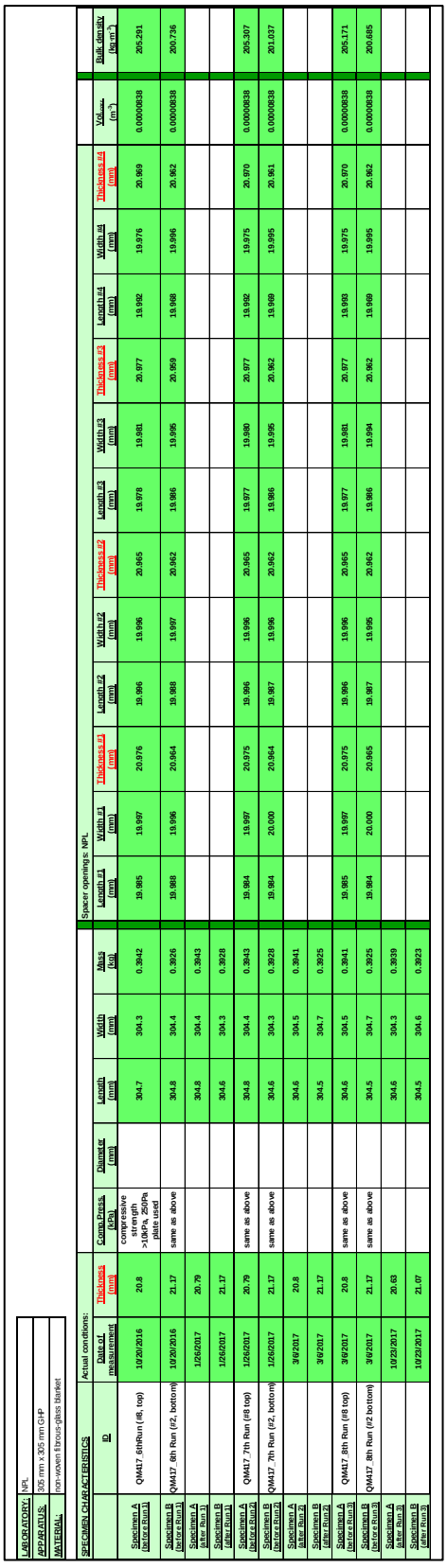

LABORATORY: NPL
APPARATUS: 305 mm x 305 mm GHP
MATERIAL: non-woven fiberous-glass blanket

SPECIMEN CHARACTERISTICS:		Actual conditions:							Spacer openings: NPL																
	ID	Date of measurement	Thickness (mm)	Comp.Press. (kPa)	Diameter (mm)	Length (mm)	Width (mm)	Mass (kg)	Length #1 (mm)	Width #1 (mm)	Thickness #1 (mm)	Length #2 (mm)	Width #2 (mm)	Thickness #2 (mm)	Length #3 (mm)	Width #3 (mm)	Thickness #3 (mm)	Length #4 (mm)	Width #4 (mm)	Thickness #4 (mm)	Vol$_{spec}$ (m^3)	Bulk density ($kg\,m^{-3}$)
Specimen A (before Run1)	QM417_6thRun (#8, top)	10/20/2016	20.8	compressive strength >10kPa, 25kPa plate used		304.7	304.3	0.3842	19.985	19.997	20.976	19.996	19.996	20.965	19.978	19.981	20.977	19.992	19.976	20.969	0.00000838	205.291
Specimen B (before Run1)	QM417_6th Run (#2, bottom)	10/20/2016	21.17	same as above		304.8	304.4	0.3826	19.988	19.996	20.964	19.988	19.997	20.962	19.986	19.995	20.969	19.988	19.996	20.962	0.00000838	200.736
Specimen A after Run1		1/26/2017	20.79			304.8	304.4	0.3843														
Specimen B after Run1		1/26/2017	21.17			304.6	304.3	0.3828														
Specimen A (before Run4	QM417_7th Run (#8 top)	1/26/2017	20.79	same as above		304.8	304.4	0.3843	19.984	19.997	20.975	19.996	19.996	20.965	19.977	19.980	20.977	19.992	19.975	20.970	0.00000838	205.307
Specimen B (before Run4	QM417_7th Run (#2, bottom)	1/26/2017	21.17	same as above		304.6	304.3	0.3828	19.984	20.000	20.964	19.987	19.996	20.962	19.986	19.995	20.962	19.989	19.995	20.961	0.00000838	201.037
Specimen A after Run2		3/6/2017	20.8			304.6	304.5	0.3841														
Specimen B after Run2		3/6/2017	21.17			304.5	304.7	0.3825														
Specimen A (before Run3	QM417_8th Run (#8 top)	3/6/2017	20.8	same as above		304.8	304.5	0.3841	19.985	19.997	20.975	19.996	19.996	20.965	19.977	19.981	20.977	19.993	19.975	20.970	0.00000838	205.171
Specimen B (before Run3	QM417_8th Run (#2 bottom)	3/6/2017	21.17	same as above		304.5	304.7	0.3825	19.984	20.000	20.965	19.987	19.995	20.962	19.986	19.994	20.962	19.989	19.995	20.962	0.00000838	200.685
Specimen A after Run3		10/23/2017	20.63			304.6	304.3	0.3839														
Specimen B after Run3		10/23/2017	21.07			304.5	304.6	0.3823														

Fig. 22. NPL specimen data.

Appendix C: Guarded-Hot-Plate Measurements – Report Form

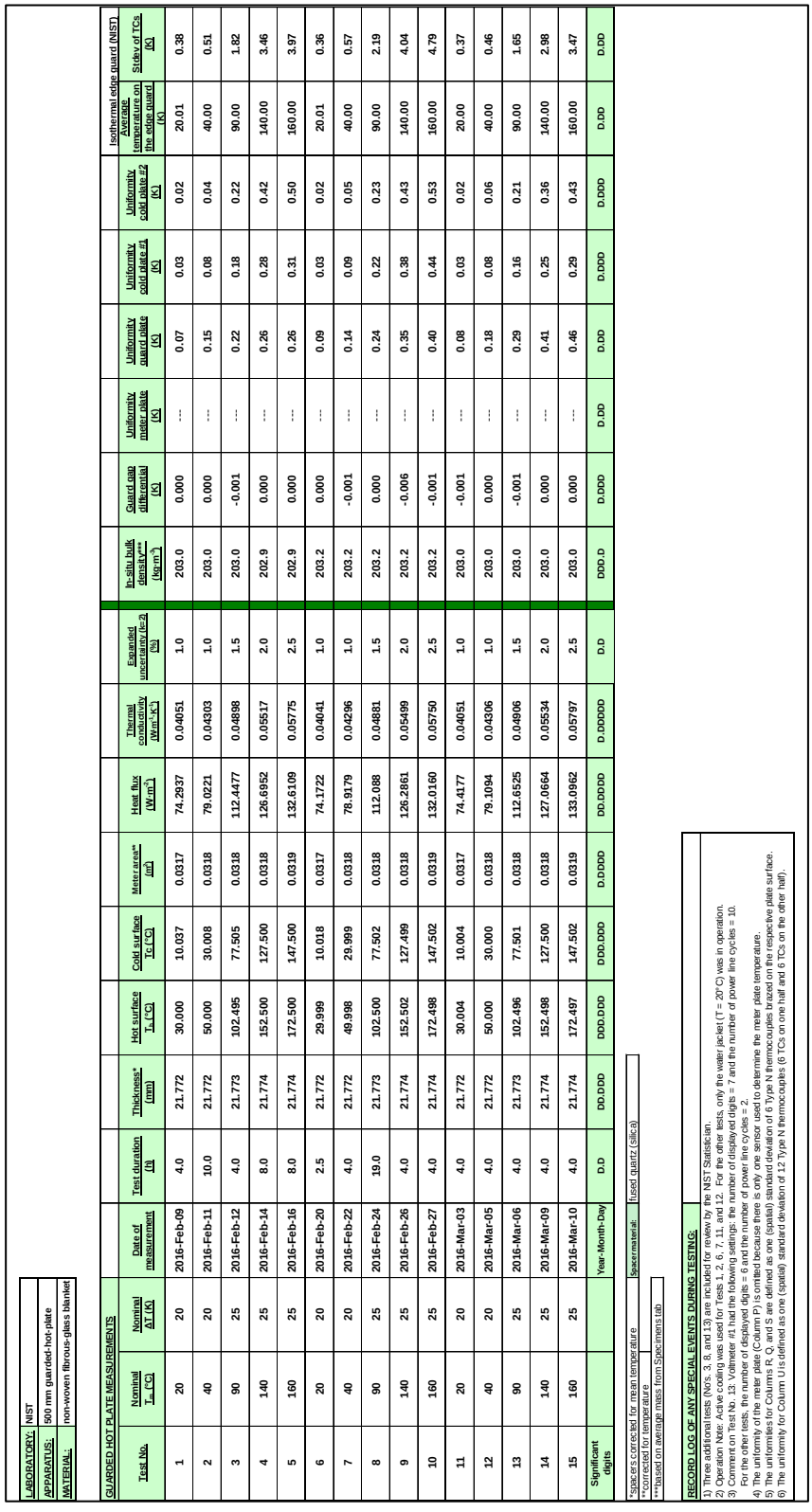

LABORATORY:	NIST
APPARATUS:	500 mm guarded-hot-plate
MATERIAL:	non-woven fibrous-glass blanket

GUARDED HOT PLATE MEASUREMENTS

Test No.	Nominal T_m (°C)	Nominal ΔT (K)	Date of measurement	Test duration (h)	Thickness* (mm)	Hot surface T_h (°C)	Cold surface T_c (°C)	Meter area** (m^2)	Heat flux ($W·m^{-2}$)	Thermal conductivity ($W·m^{-1}·K^{-1}$)	Expanded uncertainty (k=2) (%)	In-situ bulk density*** ($kg·m^{-3}$)	Guard gap differential (K)	Uniformity inside plate (K)	Uniformity around plate (K)	Uniformity cold plate #2 (K)	Uniformity cold plate #1 (K)	Isothermal edge guard (NIST) Average temperature on the edge guard (K)	Stdev of TCs (K)
1	20	20	2016-Feb-09	4.0	21.772	30.000	10.037	0.0317	74.2937	0.04051	1.0	203.0	0.000	---	0.07	0.03	0.02	20.01	0.38
2	40	20	2016-Feb-11	10.0	21.772	50.000	30.008	0.0318	79.0221	0.04303	1.0	203.0	0.000	---	0.15	0.08	0.04	40.00	0.51
3	90	25	2016-Feb-12	4.0	21.773	102.495	77.505	0.0318	112.4477	0.04898	1.5	203.0	-0.001	---	0.22	0.18	0.22	90.00	1.82
4	140	25	2016-Feb-14	8.0	21.774	152.500	127.500	0.0318	126.6952	0.05517	2.0	202.9	0.000	---	0.26	0.28	0.42	140.00	3.46
5	160	25	2016-Feb-16	8.0	21.774	172.500	147.500	0.0319	132.6109	0.05775	2.5	202.9	0.000	---	0.26	0.31	0.50	160.00	3.97
6	20	20	2016-Feb-20	2.5	21.772	29.999	10.018	0.0317	74.1722	0.04041	1.0	203.2	0.000	---	0.09	0.03	0.02	20.01	0.36
7	40	20	2016-Feb-22	4.0	21.772	49.998	29.999	0.0318	78.9179	0.04296	1.0	203.2	-0.001	---	0.14	0.09	0.05	40.00	0.57
8	90	25	2016-Feb-24	19.0	21.773	102.500	77.502	0.0318	112.088	0.04881	1.5	203.2	0.000	---	0.24	0.22	0.23	90.00	2.19
9	140	25	2016-Feb-26	4.0	21.774	152.502	127.499	0.0318	126.2861	0.05499	2.0	203.2	-0.006	---	0.35	0.38	0.43	140.00	4.04
10	160	25	2016-Feb-27	4.0	21.774	172.498	147.502	0.0319	132.0160	0.05750	2.5	203.2	-0.001	---	0.40	0.44	0.53	160.00	4.79
11	20	20	2016-Mar-03	4.0	21.772	30.004	10.004	0.0317	74.4177	0.04051	1.0	203.0	-0.001	---	0.08	0.03	0.02	20.00	0.37
12	40	20	2016-Mar-05	4.0	21.772	50.000	30.000	0.0318	79.1094	0.04306	1.0	203.0	0.000	---	0.18	0.08	0.06	40.00	0.46
13	90	25	2016-Mar-06	4.0	21.773	102.496	77.501	0.0318	112.6525	0.04906	1.5	203.0	-0.001	---	0.29	0.16	0.21	90.00	1.65
14	140	25	2016-Mar-09	4.0	21.774	152.498	127.500	0.0318	127.0664	0.05534	2.0	203.0	0.000	---	0.41	0.25	0.36	140.00	2.98
15	160	25	2016-Mar-10	4.0	21.774	172.497	147.502	0.0319	133.0962	0.05797	2.5	203.0	0.000	---	0.46	0.29	0.43	160.00	3.47
Significant digits			Year-Month-Day	D.D	DD.DDD	DDD.DDD	DDD.DDD	D.DDDD	DD.DDDD	D.DDDDD	D.D	DDD.D	D.DDD	D.DD	D.DD	D.DDD	D.DDD	D.DD	D.DD

*spacer is corrected for mean temperature. Spacer material: fused quartz (silica)

**corrected for temperature.

***based on average mass from Specimens tab

RECORD LOG OF ANY SPECIAL EVENTS DURING TESTING:

1) Three additional tests (No's. 3, 8, and 13) are included for review by the NIST Statistician.
2) Operation Note: Active cooling was used for Tests 1, 2, 6, 7, 11, and 12. For the other tests, only the water jacket (T = 20°C) was in operation.
3) Comment on Test No. 13: Voltmeter #1 had the following settings: the number of displayed digits = 7 and the number of power line cycles = 10. For the other tests, the number of displayed digits = 6 and the number of power line cycles = 2.
4) The uniformity of the meter plate (Column P) is omitted because there is only one sensor used to determine the meter plate temperature.
5) The uniformities for Columns R, Q, and S are defined as one (spatial) standard deviation of 6 Type N thermocouples brazed on the respective plate surface.
6) The uniformity for Column U is defined as one (spatial) standard deviation of 12 Type N thermocouples (6 TCs on one half and 6 TCs on the other half).

Fig. 23. NIST guarded-hot-plate measurement data.

Appendix C

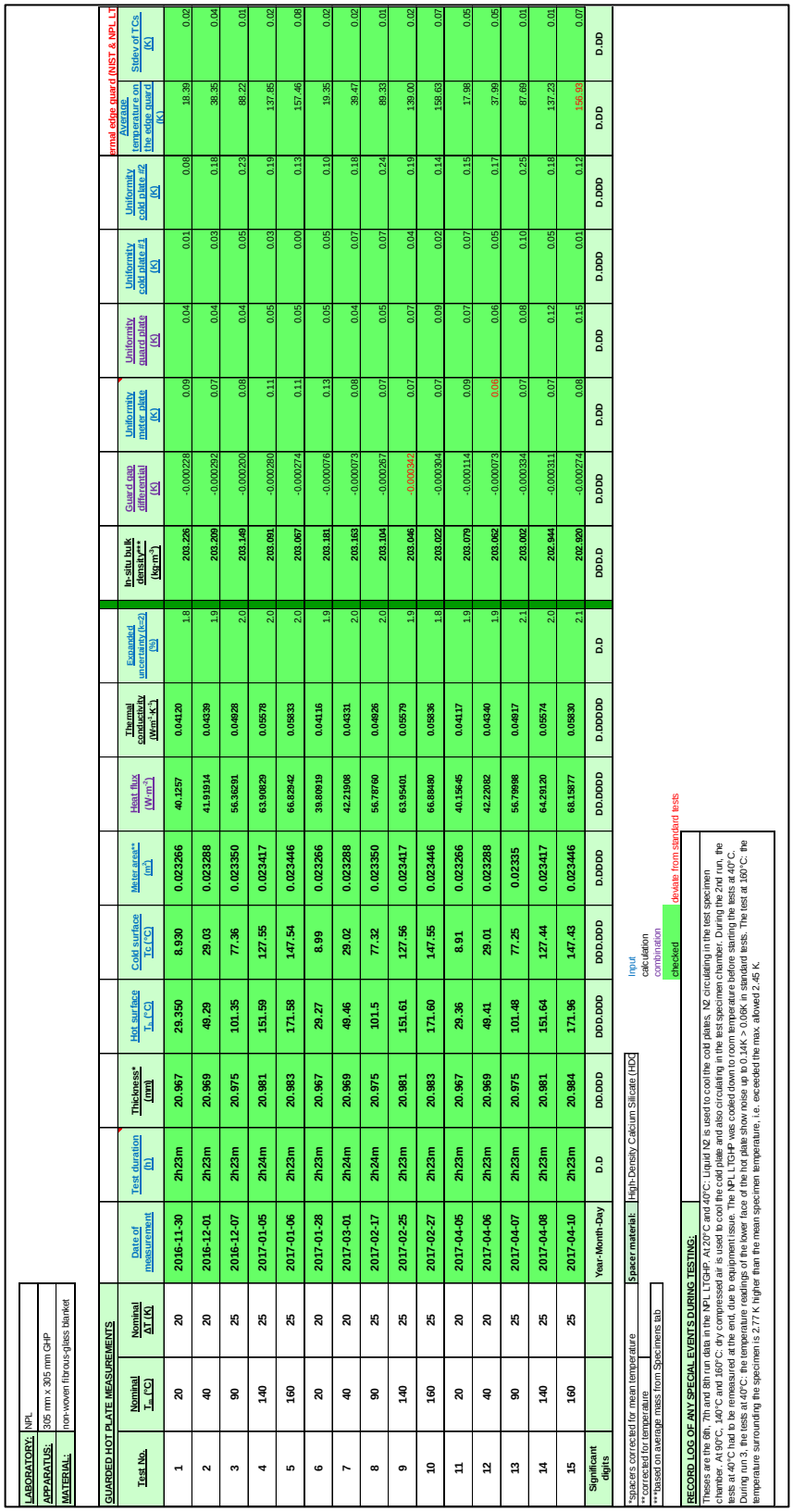

LABORATORY: NPL
APPARATUS: 305 mm x 305 mm GHP
MATERIAL: non-woven fibrous-glass blanket

GUARDED HOT PLATE MEASUREMENTS

Test No.	Nominal T_m (°C)	Nominal ΔT (K)	Date of measurement	Test duration (h)	Thickness* (mm)	Hot surface T_h (°C)	Cold surface T_c (°C)	Meter area** (m^2)	Heat flux ($W·m^{-2}$)	Thermal conductivity ($W·m^{-1}·K^{-1}$)	Expanded uncertainty (k=2) (%)	In-situ bulk density*** ($kg·m^{-3}$)	Guard gap differential (K)	Uniformity meter plate (K)	Uniformity guard plate (K)	Uniformity cold plate #1 (K)	Uniformity cold plate #2 (K)	Average temperature on the edge guard (K)	Stdev of TCs (K)
1	20	20	2016-11-30	2h23m	20.967	29.350	8.930	0.023266	40.1257	0.04120	1.8	203.226	-0.000228	0.09	0.04	0.01	0.08	18.39	0.02
2	40	20	2016-12-01	2h23m	20.969	49.29	29.03	0.023288	41.91914	0.04339	1.9	203.209	-0.000292	0.07	0.04	0.03	0.18	38.35	0.04
3	90	25	2016-12-07	2h23m	20.975	101.35	77.36	0.023350	56.36291	0.04928	2.0	203.149	-0.000200	0.08	0.04	0.05	0.23	88.22	0.01
4	140	25	2017-01-05	2h24m	20.981	151.59	127.55	0.023417	63.90829	0.05578	2.0	203.091	-0.000280	0.11	0.05	0.03	0.19	137.86	0.02
5	160	25	2017-01-06	2h23m	20.983	171.58	147.54	0.023446	66.82942	0.05833	2.0	203.067	-0.000274	0.11	0.05	0.00	0.13	157.46	0.08
6	20	20	2017-01-28	2h23m	20.967	29.27	8.99	0.023266	39.80919	0.04116	1.9	203.181	-0.000076	0.13	0.05	0.05	0.10	19.35	0.02
7	40	20	2017-03-01	2h24m	20.969	49.46	29.02	0.023288	42.21908	0.04331	2.0	203.163	-0.000073	0.08	0.04	0.07	0.18	39.47	0.02
8	90	25	2017-02-17	2h24m	20.975	101.5	77.32	0.023350	56.78760	0.04926	2.0	203.104	-0.000267	0.07	0.05	0.07	0.24	89.33	0.01
9	140	25	2017-02-25	2h23m	20.981	151.61	127.56	0.023417	63.95401	0.05579	1.9	203.046	-0.000342	0.07	0.07	0.04	0.19	139.00	0.02
10	160	25	2017-02-27	2h23m	20.983	171.60	147.55	0.023446	66.88480	0.05836	1.8	203.022	-0.000304	0.07	0.09	0.02	0.14	159.69	0.07
11	20	20	2017-04-05	2h23m	20.967	29.36	8.91	0.023266	40.15645	0.04117	1.9	203.079	-0.000114	0.09	0.07	0.07	0.15	17.98	0.05
12	40	20	2017-04-06	2h23m	20.969	49.41	29.01	0.023288	42.22082	0.04340	1.9	203.062	-0.000073	0.06	0.06	0.05	0.17	37.99	0.05
13	90	25	2017-04-07	2h23m	20.975	101.48	77.25	0.02335	56.79988	0.04917	2.1	203.002	-0.000334	0.07	0.08	0.10	0.25	87.69	0.01
14	140	25	2017-04-08	2h23m	20.981	151.64	127.44	0.023417	64.29120	0.05574	2.0	202.944	-0.000311	0.07	0.12	0.05	0.18	137.23	0.01
15	160	25	2017-04-10	2h23m	20.984	171.96	147.43	0.023446	68.15877	0.05830	2.1	202.920	-0.000274	0.08	0.15	0.01	0.12	156.93	0.07
Significant digits			Year-Month-Day	D.D	DD.DDD	DDD.DDD	DDD.DDD	D.DDDD	DD.DDDD	D.DDDDD	D.D	DDD.D	D.DDD	D.DD	D.DD	D.DDD	D.DDD	D.DDD	D.DD

Spacers corrected for mean temperature — Spacer material: High-Density Calcium Silicate (HDS)
*corrected for temperature
**based on average mass from Specimens tab

Input
calculation
combination
checked
deviate from standard tests

RECORD LOG OF ANY SPECIAL EVENTS DURING TESTING:
Theses are the 6th, 7th and 8th run data in the NPL LTGHP. At 20°C and 40°C: Liquid N2 is used to cool the cold plates. N2 circulating in the test specimen chamber. At 90°C, 140°C and 160°C: dry compressed air is used to cool the cold plate and also circulating in the test specimen chamber. During the 2nd run, the tests at 40°C had to be remeasured at the end, due to equipment issue. The NPL LTGHP was cooled down to room temperature before starting the tests at 40°C. During run 3, the tests at 40°C, the temperature readings of the lower face of the hot plate show noise up to 0.14K > 0.06K in standard tests. The test at 160°C, the temperature surrounding the specimen is 2.77 K higher than the mean specimen temperature, i.e. exceeded the max. allowed 2.45 K.

Fig. 24. NPL guarded-hot-plate measurement data.

Appendix D: Environment Measurements – Report Form

LABORATORY:	NIST					
APPARATUS:	500 mm guarded-hot-plate					
MATERIAL:	non-woven fibrous-glass blanket					
MEASUREMENT ENVIRONMENT CONDITIONS						NIST
Test No.	Nominal T_m (°C)	Nominal ΔT (K)	Date of measurement	Ambient temperature (°C)	Ambient pressure (kPa)	Ambient dewpoint (°C)
1	20	20	2016-Feb-09	21.46	98.24	-69
2	40	20	2016-Feb-11	23.34	99.65	-73
3	90	25	2016-Feb-12	28.08	99.84	-74
4	140	25	2016-Feb-14	32.70	101.46	-75
5	160	25	2016-Feb-16	34.83	98.63	-70
6	20	20	2016-Feb-20	18.85	99.38	-66
7	40	20	2016-Feb-22	21.54	100.20	-65
8	90	25	2016-Feb-24	27.04	98.67	-66
9	140	25	2016-Feb-26	32.06	99.45	-68
10	160	25	2016-Feb-27	34.21	100.04	-71
11	20	20	2016-Mar-03	19.25	100.40	-71
12	40	20	2016-Mar-05	20.83	100.45	-70
13	90	25	2016-Mar-06	27.13	100.69	-69
14	140	25	2016-Mar-09	32.30	100.30	-67
15	160	25	2016-Mar-10	34.32	99.90	-65
Significant digits			Year-Month-Day	DD.DD	DDD.DD	DD

Fig. 25. NIST environmental data.

Appendix D

LABORATORY:	NPL
APPARATUS:	305 mm x 305 mm GHP
MATERIAL:	non-woven fibrous-glass blanket

MEASUREMENT ENVIRONMENT CONDITIONS						NPL
Test No.	Nominal T_m (°C)	Nominal ΔT (K)	Date of measurement	Ambient temperature (°C)	Ambient pressure (kPa)	Ambient humidity (%RH)
1	20	20	2016-11-30	22.90	103.39	14.5
2	40	20	2016-12-01	22.60	103.072	14.4
3	90	25	2016-12-07	24.85	102.525	33.95
4	140	25	2017-01-05	22.54	103.093	18.52
5	160	25	2017-01-06	22.50	103.585	19.2
6	20	20	2017-01-28	22.78	100.568	22.9
7	40	20	2017-03-01	22.50	99.569	27.24
8	90	25	2017-02-17	24.12	102.653	30.52
9	140	25	2017-02-25	23.42	101.520	29.5
10	160	25	2017-02-27	23.40	99.193	34.2
11	20	20	2017-04-05	22.26	102.983	28.76
12	40	20	2017-04-06	22.42	103.003	29.7
13	90	25	2017-04-07	22.82	102.713	29.2
14	140	25	2017-04-08	22.62	102.354	31.28
15	160	25	2017-04-10	22.72	102.092	33.62
Significant digits			Year-Month-Day	DD.DD	DDD.DD	DD

Fig. 26. NPL environmental data.